TRANSCRIPTOMICS PROFILING OF M6A RNA MODIFICATIONS IN TNF-ALPHA INDUCED APOPTOSIS

A Thesis Submitted to
the Graduate School of Engineering and Sciences of
İzmir Institute of Technology
in Partial Fulfillment of the Requirements for the Degree of

MASTER OF SCIENCE

in Molecular Biology and Genetics

by
Azime AKÇAÖZ

December 2021

İZMİR

ACKNOWLEDGEMENTS

My deep gratitude goes first to my supervisor Prof. Dr. Bünyamin AKGÜL for his continued support, encouragement, inspirations, and comments throughout the course of the project. I want to indicate my thanks and regards to TUBITAK (Scientific and Technological Research Council of Turkey) due to their support and fund. (Project No: 217Z234).

I would like to express my special thanks to my committee members Assoc. Prof. Dr. Özden YALÇIN-ÖZUYSAL and Prof. Dr. Uygar Halis TAZEBAY for their valuable time and comments to support my thesis.

I am also deeply thankful to Dr. İpek ERDOĞAN and Özge TÜNCEL for her valuable technical support, friendship, patience, and guidance. I extend my gratitude to my other colleagues, Merve KARA, Melis ATBİNEK, Buket SAĞLAM, Bilge YAYLAK, Ayşe Bengisu GELMEZ, Dilek Cansu GÜRER, and Vahide İlayda KAÇAR for their help in dealing with experiments. I cannot thank enough to my student Yasemin GAZLAOĞLU for her interests, help, and friendship. I am also thankful to Biotechnology and Bioengineering Central Research specialists Özgür AKIN for her sincere help and kindness during my studies.

Special thanks should be given to Başak ÇOBAN and Erhan ALASAR for their support, motivation, and faith during my graduate life. I wish to declare my deepest thanks to my family.

ABSTRACT

TRANSCRIPTOMICS PROFILING OF m^{6}A RNA MODIFICATIONS IN TNF-ALPHA INDUCED APOPTOSIS

Apoptosis is a form of programmed cell death that occurs as a result of physiological or pathological causes. TNF-alpha, which has a regulatory role in immune system cells, stimulates apoptosis through the external pathway. For this reason, it can be used for the treatment of various diseases. Although there are many studies on the regulatory mechanisms of TNF-alpha mediated apoptosis, the contribution of RNA modifications has not been fully elucidated. Regarding the potential role of m^{6}A RNA modification in apoptosis, studies have focused on the effects of regulatory proteins and there is no genome-wide m^{6}A methylation profile yet. In the present thesis, firstly, the gene expression patterns of m^{6}A writer, eraser, and reader were examined in HeLa cells and 632 genes with differential m^{6}A methylation pattern were identified by the miCLIP method. 99 genes involved in apoptotic pathways were determined by GO analysis. Candidates were selected based on m6A methylation fold change, intracellular expression level and apoptotic role of the relevant gene. Methylation points in IGV were confirmed and specific validation experiments were performed on these m^{6}A points. SELECT based validation studies showed 1-2 cycle increase in the TNF-alpha group compared to the control group. This confirms the miCLIP data, which also pointed to an increase in m^{6}A methylation. To elucidate the fate of candidate RNAs, the gene expression levels, and translational status of candidate genes were analyzed. METTL3 KD HeLa cells exposed to TNF-alpha exhibited an increase in the expression of PHLDA1, IFI6 and HRK by almost 2-fold. Polysome fractionation assay showed that translation level decreased in TNF-alpha treated METTL3 KD HeLa cells. As a conclusion, global m6A level affected RNA abundance as well as translation.

Keywords: *Apoptosis, TNF-alpha, m^{6}A RNA Modification, miCLIP, SELECT*

ÖZET

TNF ALFA İLE İNDÜKLENMİŞ APOPTOZDA M^6A RNA MODİFİKASYONLARININ TRANSKRİPTOMİK PROFİLLENMESİ

Apoptoz fizyolojik ya da patolojik sebepler sonucu meydana gelen programlı hücre ölümüdür. İç ya da dış yolaklar sonucu meydana gelen bu hücre ölümünde, bağışıklık sistemi hücrelerini düzenleyici görevi olan TNF alfa dış yolaktan apoptozu uyarmaktadır. Bu sebeple çeşitli hastalıkların tedavisinde kullanılabilmektedir. TNF alfanın apoptozu tetiklemesindeki düzenleyici mekanizmaları üzerine birçok çalışma mevcut olmakla birlikte RNA modifikasyonlarının bu sistemdeki düzenleyici mekanizması tam olarak aydınlatılmamıştır. Ayrıca, apoptoz ve mRNA'larda sık olarak görülen m^6A RNA modifikasyonu ile ilgili olarak çalışmalar düzenleyici proteinlerin etkilerine odaklanmış olup genom kapsamlı bir m^6A metilasyonu taraması bulunmamaktadır. Bu sebeple, mevcut tez çalışmasında öncelikle TNF alfa ile apoptoz tetiklenmiş HeLa hücrelerinde m^6A metilasyonundan sorumlu yazıcı, silici ve okuyucu proteinlerin gen ekspresyonları taranmış ve m^6A metilasyonu artan/azalan 632 gen miCLIP yöntemi ile tanımlanmıştır. GO analizi ile apoptotik yolaklarda rol alan 99 tane gen belirlenmiştir. İlgili genin m^6A metilasyonu artış kat sayısı, hücre içi ekspresyon seviyesi ve apoptotik rolü baz alınarak seçilen adaylar için öncelikle IGV'de metilasyon noktaları doğrulanmış ve daha sonra bu noktalara spesifik validasyon deneyi gerçekleştirilmiştir. SELECT sonucunda TNF alfa grubunda kontrol grubuna göre 1-2 döngülük artış tespit edilmiştir. Bu da m^6A metilasyonunda artış olduğunu göstererek miCLIP datasını doğrulamaktadır. Metilasyonun RNA kaderine etkisinin analizinde, TNF-alpha uygulanan METTL3 susturulmuş hücrelerde PHLDA1, IFI6, HRK ve GADD45B ekspresyon seviyelerinde artış gözlemlendi. Translasyonel seviye ise polizom fraksiyon analizi ile incelendi. Sonuç olarak, global m6A metilasyon seviyesindeki değişimin hem RNA seviyesine hem de translasyon seviyesine etki ettiği gözlemlendi.

Anahtar Kelimeler: *Apoptoz, TNF-alfa, m^6A RNA Modifikasyonu, miCLIP, SELECT*

TABLE OF CONTENTS

LIST OF FIGURES

Figures **Pages**

Figures **Pages**

LIST OF TABLES

Tables **Pages**

CHAPTER 1

INTRODUCTION

Regulated cell death (RCD) is a biologically controlled process involving genetically defined molecular mechanisms and signaling cascades (Tang et al. 2019). RCD is a type of cell death which has been described by the Nomenclature Committee on Cell Death (NCCD) based on morphological, functional, and biochemical properties. The regulation of RCD is important for pathological and physiological processes such as homeostasis or tumorigenesis (Galluzzi et al. 2015). It requires more research to define the critical role of excessive or deficient RCD in human disease. NCCD defined programmed cell death (PCD) as a part of RCD in 2015 and 12 cell death programs have been described including apoptosis, necrosis, autophagy and ferroptosis, all of which have specific morphological differences (Galluzzi et al. 2015; Del Re et al. 2019).

1.1. Apoptosis

Apoptosis is considered as a distinctive and important type of PCD, which results in elimination of cells through a series of biochemical events occurring in the cell (Elmore 2007; Pistritto et al. 2016). It was firstly coined by Kerr et al. in 1972 after they detected some morphological changes such as cytoplasmic shrinkage, chromatin condensation, nuclear fragmentation, blebbing and apoptotic bodies in the dying cells. In apoptotic cells undergoing these morphological changes, apoptotic bodies which include cytoplasm with highly packed organelles and genomic fragments are phagocytosed by macrophages, parenchymal or neoplastic cells without any inflammation (Kerr J. F. R., Wyllie A. H. 1972; Kurosaka et al. 2003).

Apoptosis can be triggered by some physiologic cues, such as maintenance of homeostasis, developmental processes, elimination of pathogen-invaded cells and death

of immune cells that have completed their function, as well as pathologic factors, such as DNA damage due to radiation, ER stress caused by accumulation of misfolded proteins and some conditions like autoimmune diseases, neurodegeneration or cancer (Kaczanowski 2016). Therefore, the elucidation of apoptosis at the molecular level has high importance.

1.2. Mechanism of apoptosis

Apoptotic mechanisms can be dependent on or independent of caspases, a family of cysteine proteases (Julien and Wells 2017). Caspase-dependent process consist of two major distinct pathways,instrinsic and extrinsic pathways in addition to perforin/granzyme pathway. All of these pathways involve the cleavage of caspases and formation of an apoptotic machinery. The perforin/granzyme pathway metiated by cytototix T cells or natural killer cells begins with secretion of granules containing granzyme A and B. They can easily pass through the pores of target cells. Granzyme B promotes indirect caspase activation via pro-apoptotic BH3 proteins wheares granzyme A can cleave nuclear proteins resulting in single-strand DNA breaks (Figure 1) (Sivamani 2015; Klanova and Klener 2020).

Many extracellular or intracellular stimuli activate the intrinsic apoptotic pathway mediated by mitochondria such as toxins, radiation, oxidative stress or treatment with chemotherapeutic agents (Sivamani 2015; Pistritto et al. 2016). The functional outcome of pro-apoptotic signaling of the BAX and BAK is neutralization of anti-apoptotic proteins such as BCL-2, BCL-XL and MCL-1. It promotes mitochondria outer membrane permeabilization (MOMP) resulting in release of cytochrome c which has a key role in activation of mitochondrial-dependent death in cytoplasm. The cytochrome c interacts with APAF-1 to form apoptosome structure which recruits pro-initiator caspase-9. The oligomerization of caspase-9 on the apoptosome allows auto-cleavage. Then, active caspase-9 activates caspase-3, -6 and -7 (Figure 1). The signaling caspase cascade leads to the demolition of cells and ends up with apoptosis (G. Xu and Shi 2007; Jan and Chaudhry 2019; Pistritto et al. 2016; Sivamani 2015).

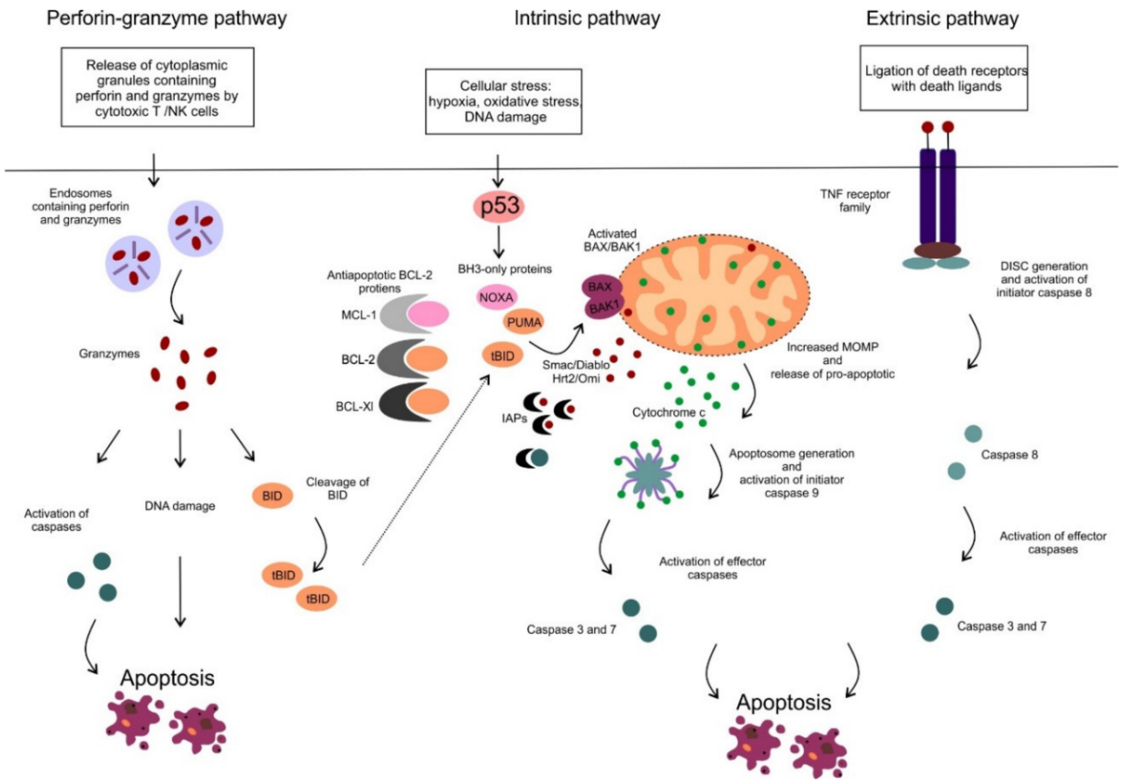

Figure 1.5. Caspase-dependent apoptotic pathways.

(Klanova and Klener 2020)

In extrinsic pathway, the stimulation of transmembrane death receptor after binding of death ligands triggers apoptosis. Death receptors are structurally characterized by intracellular motifs such as death domain (DD) and death effector domain (DED). Pro-apoptotic death receptors include tumor necrosis factor (TNF) receptors, which are TNF-R1 and TNF-R2, TNF-related apoptosis-inducing ligand (TRAIL) receptors including TRAIL-R1 and TRAIL-R2, FAS, DR4 and DR5 (Sivamani 2015; Jan and Chaudhry 2019; Carneiro and El-Deiry 2020).

Apoptotic signaling through the extrinsic pathway requires extracellular ligands such as TNFα, Fas ligand (Fas-L) or TRAIL. Upon the binding of ligand to its corresponding death receptor, trimerization and aggregation of receptors occur to expose DD-interactions by a conformational change (Jan and Chaudhry 2019). This is followed by formation of death including signaling complex (DISC) as a result of recruitment of adaptor proteins FADD/TRADD and initiator caspase -8 and -10. DISC promotes auto-

activation of caspase-8 and -10 leading to cleavage of effector caspases, -3, -6 and -7 (Figure 1). Thus, apoptosis is triggered by effector caspases to cleave essential substrate for cell viability (Carneiro and El-Deiry 2020; Pistritto et al. 2016).

The final step for all caspase dependent apoptotic pathways is execution pathway. The active effector caspases lead to degradation of the nuclear material by stimulating cytoplasmic endonucleases and they also activate proteases to break down nuclear and cytoskeletal proteins such as the nuclear protein NuMA and plasma membrane cytoskeletal protein alpha fodrin (PARP). All processes cause a change in the morphological and biochemical structure of the cells (Elmore 2007).

1.3. TNFα induced apoptosis

TNFα is a highly multifunctional cytokine promoting cell death and cell survival mechanisms. sTNF, secreted form of TNFα, is expressed by various cell types including macrophages and natural killer cells. TNFα is a 17-kDa protein and a soluble variant is formed by cleavage of type II single spanning transmembrane protein expressed in cell membrane (mTNF) (Horssen, Hagen, and Eggermont 2006; Wajant and Siegmund 2019). It is able to signal through two distinct transmembrane receptors TNFR-1 (p60) and TNFR-2 (p80). The binding efficiency of ligand to receptors differs. Despite the high affinity of TNF-alpha for TNFR-2, TNFR-1 executes the cell death signaling (Wajant and Siegmund 2019). Although TNFR-1 and -2 have same extracellular domains, their cytoplasmic domains have structurally different homology. TNFR-1 has DD facilitating protein-protein interaction, which is critical for apoptosis, whereas TNFR-2 devoid of a DD motif. TNFR-1 not only induces apoptosis via cytotoxic signaling pathway but also is able to activate the NF-κB pathway for cell survival. Which signaling pathway to be transduced by TNFR-1 is determined by the cell type, the state of activation of the cell and the cell cycle (Gupta 2005; Macewan 2002).

TNFR-1 and TNFR-2 have similar extracellular binding sites for sTNF and mTNF, but they induce different adaptor proteins because of their distinct intracellular structures. Upon binding of mTNF to TNFR-2, apoptosis can be stimulated directly or by the activation of ligand-passing mechanism. Due to TNFR's greater affinity and

capability of holding ligand, the concentration of mTNF and sTNF increases. Therefore, TNFR-1 binds more TNF ligands via TNFR-2, resulting in activation of apoptotic machinery by both pathways (Macewan 2002; Holbrook et al. 2019). TNFR-1 stimulation continues with conformational change in DD, allowing recruitment of TRADD and receptor interacting serine/threonine protein kinase 1 (RIPK1). It forms membrane bound complex I for cell survival, or cytoplasmic free complexes which are complex IIb inducing apoptosis and complex IIc related with necrosis. Here, which pathway will be induced is determined by ubiquitination status of RIPK1 (Holbrook et al. 2019). When RIPK1 is ubiquitinated, complex I is formed, which is composed of the adaptor TRADD, the kinase RIPK1 and TRAF2. The activation of complex II relies on the unubiquitination of RIPK1. In this complex, TRADD and RIPK1 associate with FADD in order to free DD of TRADD after its dissociation from TNFR1(Figure 2). It promotes the recruitment of pro-caspases 8. Its cleavage to caspase 8 triggers the caspase signaling cascade. The important step in this type of apoptosis is cleavage of RIPK1 by a caspase complex with cFLIP. If RIPK1 remains uncleaved, its aggregation which causes induction of necrosis via formation of complex IIc (Sedger and McDermott 2014; Rath and Aggarwal 1999; Micheau and Tschopp 2003).

1.4. Regulation of Apoptosis

Proteomics, biochemical and genetic studies demonstrated that the expression of more than a hundred proteins change in an apoptosis-induced cell in addition to a number of key regulatory proteins that play a critical role in the regulation of apoptosis. The intracellular concentrations of these regulatory proteins ultimately determine the course of apoptosis (Budhidarmo and Day 2015; R. S. Hotchkiss et al. 2009). Transcriptional regulation of all these mechanisms can progress under the control of a number of signal transduction pathways such as NF-KB, PI3K, JNK and Notch, depending on cell and tissue type and phenotype (Arya et al. 2015). Post-transcriptional mechanisms (such as RNA-binding proteins) may likewise be responsible for the regulation of these regulatory proteins. Recently, it has been shown that genes can be regulated by not only RNA-binding proteins but also non-coding RNAs. Studies indicate that both intrinsic and

extrinsic apoptotic pathways are regulated by a series of miRNAs or long non-coding RNAs (Guttman and Rinn 2012). In addition to the regulation of genes by proteins or long non-coding RNAs, one of the most exciting developments in post-transcriptional gene regulation in recent years is RNA modifications. Similar to DNA/protein modifications, RNA modifications dictate the fate of the relevant RNA in the post-transcription stage and thus can seriously affect the contribution of the relevant gene to the phenotype.

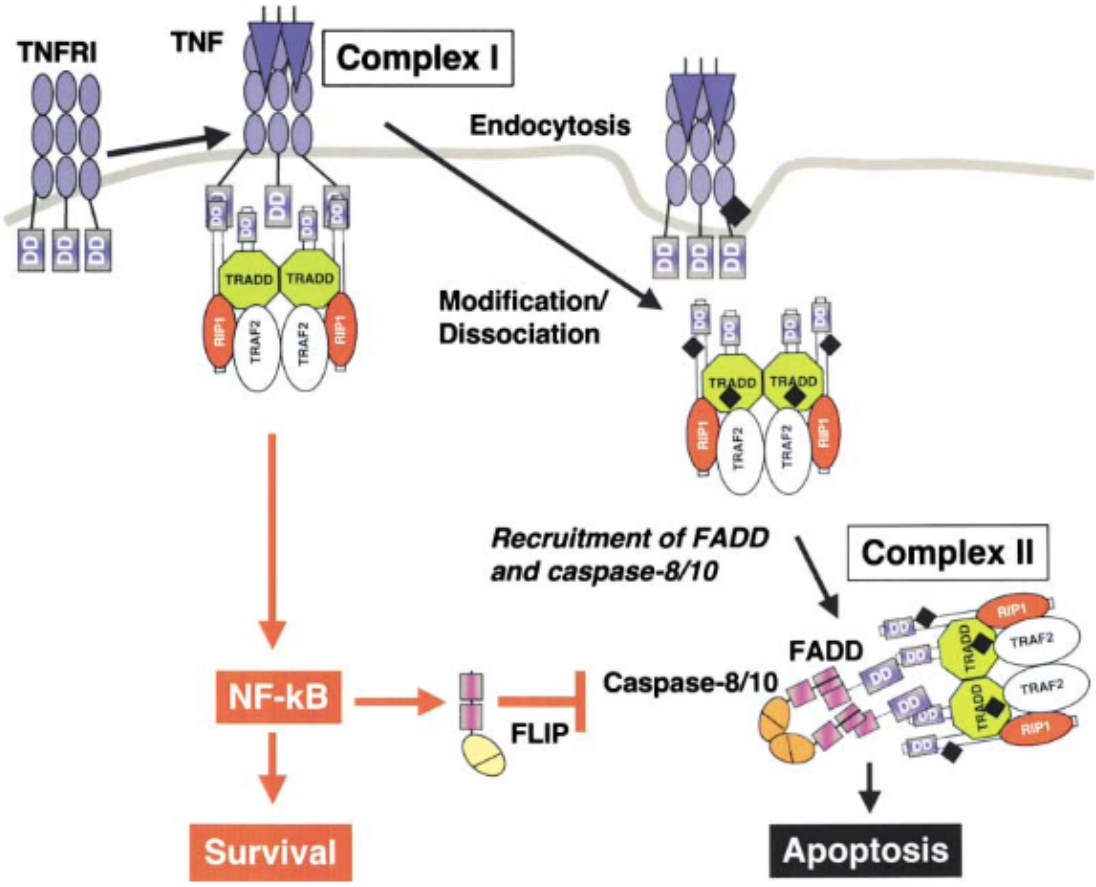

Figure 1.6. The mechanism of TNF-alpha induced apoptosis.
(Micheau and Tschopp 2003)

1.5. Epitranscriptomics

DNA and RNA molecules were thought to contain only canonical nucleotides until the discovery of deoxy 5-methylcytosine, identified in 1948 (D. Hotchkiss 1948) as the first non-canonical nucleotide on DNA. Immediately after this discovery, small structures on RNA were discovered and identified as 5-ribosyluracil in 1956 (Davis and Allen 1957) and updated as pseudouridine (Ψ) in 1960 (Cohn 1960). Shortly after the discovery of the first modification on RNA, approximately 35 more RNA modifications, such as 2'-O-methylribose, 5-methylribouridine, and 5-methylribocytosine, were reported in different studies (Grosjean 2005). The current number exceeds 150 owing to the development of RNA sequencing technology today. All these chemical RNA modifications are defined as epitranscriptomics, which is defined as functional changes in transcriptomes without any change in ribonucleotide sequence (Saletore et al. 2012). Nowadays, epitranscriptomics and epigenetics are very prominent. They are dynamic and reversible processes and can occur on any type of RNA. These modifications, thought to be on tRNAs and rRNAs at the beginning of epitranscriptomics studies, have been proven to exist on non-coding RNAs (ncRNAs) and small nuclear RNAs (snRNAs) as well as mRNAs (Cao et al. 2016). While all RNA modifications can affect RNA structure and biogenesis on rRNA and snRNAs, they may affect molecular identification in tRNAs or the regulatory information dynamics in mRNAs.(X. Wang and He 2014).

13 different modifications on mRNA are categorized into two sub-groups as cap-adjacent nucleotides and internal modifications. 7-methylguanosine (m7G), 2′-O-methylated at the ribose (cOMe) and N6,2′-O-dimethyladenosine (m^6Am) are cap-adjacent modifications that regulate mRNA stability and translation. Internal modifications occur at different position of mRNA, such as 5'untranslated region (5'UTR), 3'untranslated region (3'UTR), coding sequences (CDS) or introns. The most abundant internal mRNA modifications are N6- methyladenosine (m^6A) and adenosine to inosine (A to I) editing. Additionally, there are less abundant internal mRNA modifications such as 5-methylcytosine (m5C), pseudouridine (Ψ), N1-methyladenosine (m1A), N4-acetylcytidine (ac4C), hydroxymethylcytosine (hm5C), 3-methylcytidine (m3C), cytosine to uridine (C to U) editing, m7G, Nm, and 7,8-dihydro-8-oxoguanosine (Anreiter et al. 2021). They may play role in mRNA splicing, 3′-end processing, export,

stability, localization as well as RNA stability and translation efficiency. The modification type and location appear to dedicate the functional outcome (Nachtergaele and He 2018; Anreiter et al. 2021).

1.6. N6-Methyladenosine modification

The existence of m^6A modification was first reported in yeast rRNA and tRNAs in 1969 (Starr and Sells 1969). Subsequently, it was determined as the most common modification type in eukaryotic mRNAs in the 1970s (Desrosiers, Friderici, and Rottman 1974; Perry and Kelley 1974). It has been reported that 0.1-0.4% of all adenosines in mammals undergo m^6A methylation and it constitutes 80% of all modifications present in mRNAs (Niu et al. 2013). The m^6A residues, which are present at an average of one in 2000 ribonucleotides, are mostly enriched in 5'UTR, CDS and 3'UTR. m^6A modification only occurs in the DRACH ([G / A / U] [G> A] m^6AC [U> A> C] motif, which is a highly conserved sequence (J. Huang and Yin 2018). However, the conserved sequence flanking m^6A methylation residues may differ based on the type of RNA. However, the frequency of the conserved sequence in the genome is much higher than the m^6A modification. It means that every motif does not implicate a functional modification. Therefore, in addition to the conserved sequence, there are different factors such as RNA structure and regulatory proteins that determine the methylation point, as specific for RNA type. For example, addition of an m^6A residue on snRNAs requires the formation of a 3 'loop structure. It supports the specific regulation and function of RNA-specific methylation events (Niu et al. 2013; Wiener and Schwartz 2021).

The catalysis of m^6A methylation is carried out by adenosine methyltransferases named as writer proteins. Although a multiprotein writer complex mediates m^6A methylation on transcriptome, only METTL3 has the main catalytic activity. METTL3 harbors two functional domains for methylation process: (1) consensus methylation motif-I that contains Adomet binding site and (2) consensus motif-II which is the catalytic domain. However, METTL3 does not account for all methylation activity and the assistance of additional proteins is required (Cao et al. 2016; P. C. He and He 2021). METTL14, which is a homolog of METTL3, has a methyltransferase domain that boosts

the catalytic activity by forming a stable heterodimer with METTL3. The interface of heterodimer is 2500 A^2 and the disruption of the METTL3-METTL14 complex is extremely difficult as more than 20 amino acids interact with each other via various bonds. However, METTL14 lacks the Adomet-binding domain causing its catalytic inactivation. Despite pseudo-methyltransferase activity, METTL14 increases the binding efficiency of substrate to the binary complex by changing the structure of RNA via its positively charged groove (J. Huang and Yin 2018). The m^6A writer complex also has several regulator proteins that interact with the core complex. Wilms' tumor 1-associating protein (WTAP) mediates localization in nuclear speckles with pre-mRNA processing factors by interacting with the binary complex. WTAP also has a crucial role in the fate of RNA by regulating transcript decay or alternative splicing (Ping et al. 2014; J. Huang and Yin 2018). KIAA1429 (vir-like m^6A methyltransferase associated protein, or VIRMA), and RNA binding motif protein 15/15B (RBM15/RBM15B) are other regulatory writer proteins that interact with WTAP to specify target transcripts. Although it is known that these proteinsare the cornerstone for the writer complex, their molecular mechanisms have not been fully elucidated (Qian et al. 2019; Zaccara, Ries, and Jaffrey 2019).

RNA methylation is dynamic, rapid and signal-dependent because demethylase proteins known as erasers remove the methyl groups from methylated adenosine. AlkB homolog 5 (ALKBH5) and the fat mass and obesity- associated protein (FTO) are two fundamental erasers for m^6A modification. Even though both proteins target similar transcripts, their demethylation mechanisms are different. While ALKBH5 can directly remove the methyl group without oxidative demethylation, FTO contributes to this process in two steps (N6-hydroxymethyladenosine and N6-formyladenosine)(Cao et al. 2016). Their localization and cellular processes in which they are effective also differ. ALKBH5, which is found in nuclear speckles, play a role in gene expression, regulating export and splicing of nuclear RNA. However, FTO localizes in cytoplasm as well as nucleus and functions in mRNA splicing, cell differentiation and gene expression (Niu et al. 2013; Zaccara, Ries, and Jaffrey 2019; J. Huang and Yin 2018).

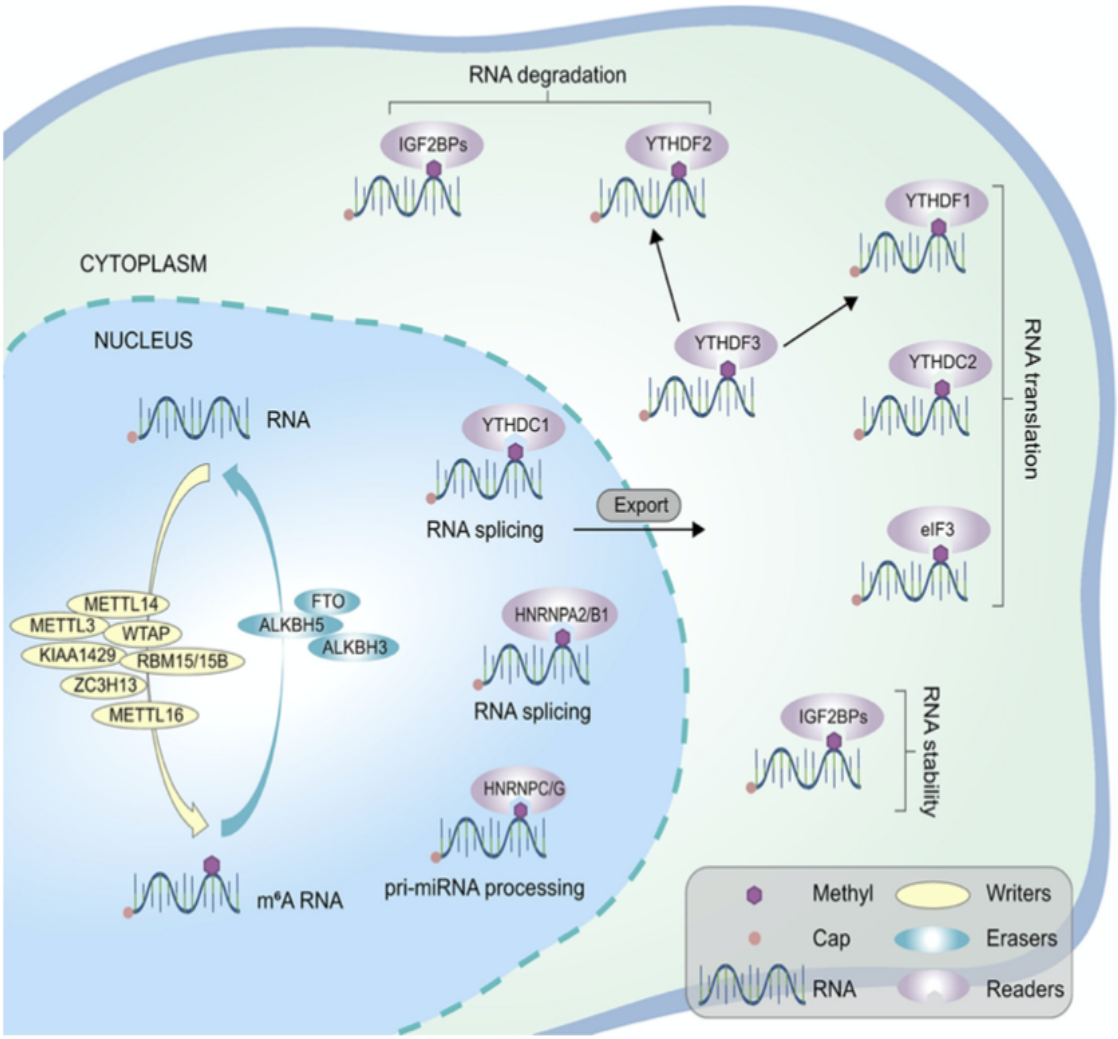

Figure 1.7. The function of m^{6}A modification determined by reader proteins. (Zhang et al. 2020)

The function of m^{6}A modification is determined by reader proteins whose mechanisms are mainly categorized into three subgroups as direct binding, m^{6}A switch and indirect binding (Zaccara, Ries, and Jaffrey 2019). YTH domain-containing proteins specifically recognize m^{6}A-methylated RNAs and consist of five members: YTHDF1, YTHDF2, YTHDF3, YTHDC1 and YTHDC2. YTHDC1 and YTHDC2 are localized in nucleus whereas YTHDF1-3 are cytosolic. However, YTHDC2 can be also found in cytoplasm and leads to mRNA degradation and the regulation of translation initiation. YTHDC1 preferentially binds non-coding RNAs as well as mRNAs and modulates their export and splicing (Kretschmer et al. 2018; Berlivet et al. 2019). YTHDFs, on the other hand, can bind to cytosolic mRNAs and cause their translation or degradation in P-bodies

(Zaccara and Jaffrey 2020). Additionally, there are studies showing that eIF3 and METTL3 can act as readers, and they enhance cap-dependent translation of their target RNAs (Shuibin Lin et al. 2016). Since m^6A-U baseparing is much weaker than A-U without methylation, it can negatively affect the folded structure of RNA and cause it to remain in a linear state named m^6A structural switch. Thus, RNA binding proteins can bind to RNA more effectively (Zaccara, Ries, and Jaffrey 2019). Heterogeneous nuclear ribonucleoprotein G (HNRNPG), an RNA-binding protein involved in splicing, and A2B1 (HNRNPA2B1) recognized the sites m^6A which are predominantly cytosolic and play role in microRNA processing by affecting splicing of non-coding RNA (J. Huang and Yin 2018). The mechanism of indirect recognition is unclear. At last group, there are FMRP, the fragile X mental retardation protein, and IGF2BP proteins (IGF2BP1, IGF2BP2 and IGF2BP3). They are localized in both nucleus and cytoplasm. IGF2BPs can bind to the m^6A motif as well as recognize different sequences, but in the case of m^6A binding, it increases the stability of mRNAs (Hu et al. 2020; H. Huang et al. 2018). FMRP, on the other hand, binds to YTHDF2 rather than directly to the methyl group and indirectly affects mRNA stability (Hsu et al. 2019).

1.7. Experimental and computational approaches for identification of m^6A modification

Since m^6A methylation does not cause any base change on the ribonucleotide sequence, it cannot be detected by second generation sequencing. For this reason, new methods are being developed continuously. These methods include antibody-based, digestion-based, and ligation-based detection approaches. In addition, various methods have been developed based on deamination, nanopore direct RNA sequencing or computational predictions (Zhu et al. 2019; Capitanchik et al. 2020).

In the m^6A-seq or MeRIP-seq method, which was first developed for transcriptome-wide profiling, next generation sequencing is performed following precipitation of methylated RNAs using m^6A antibodies (Dominissini et al. 2012). However, in this method, the exact point of methylation cannot be determined since sequencing is carried out with fragmented RNAs. To increase resolution, RNAs are

exposed to UV-crosslinking after antibody treatment to create point mutations or truncation. Therefore, m^6A individual-nucleotide-resolution cross-linking and immunoprecipitation (miCLIP) technique can efficiently identify m^6A residues. RNAs required for miCLIP are isolated from any source, then exposed to UV-crosslinking *in vitro* and then immunoprecipitation is performed. Amino acid adducts from the antibody removed with the help of Proteinase K remains attached to the RNA. During cDNA synthesis, reverse transcriptase can create a point mutation or deletion in this amino acid adduct or stop the synthesis. Then, the m^6A regions at the single nucleotide resolution are determined by computational analysis. Although this method is high throughput, it has some weaknesses. For example, eliminating nonspecific antibody binding is very difficult and also requires very high amounts of input material (Linder et al. 2015).

Various m^6A identification methods have been developed that make it possible to identify m^6A residues at single base resolution. MAZTER-seq and m^6A-REF-seq, described in 2017, can cut from the ACA motif (Imanishi et al. 2017). Unlike antibody-based methods, MAZTER-seq provides semiquantitative information and creates stoichiometric data (Capitanchik et al. 2020). In the MAZTER-seq method, isolated mRNA is treated with MazF m^6A methylation reduces the cleavage efficiency of the enzyme. The amount of methylation at the same point in all transcripts of a gene can be determined by the cut/uncut ratio. However, since only methylations in the ACA motif can be determined with MAZTER-seq, ACU and ACC motifs are disregarded, so it does not cover a genome wide profile. In addition, it requires complex bioinformatics analyses (Garcia-Campos et al. 2019).

In ligation-based methods, T3/T4 DNA ligase-qPCR was developed first. In this method, ligation efficiency is determined by qPCR using two methylation site-specific probes. Ligation does not occur in the presence of m^6A, as methylation reduces the enzyme efficiency (W. Liu et al. 2018). Although there are easy preparation steps, there is a lot of dependence on the ligation efficiency, and it is low throughput. In single-base elongation- and ligation-based qPCR amplification method (SELECT), another ligation-based method, there is a two-step selection. Two probes specific to the 15bp right and 15bp left of the target methylation are used, but T corresponding to the m^6A is not present in the probes. Ligation efficiency is measured by qPCR using Bst DNA polymerase and SplintR ligase. m6A prevents the addition of T by polymerase and ligation by SplintR ligase even if T is added (Xiao et al. 2018). With SELECT, m^6A stoichiometry can be

measured and at the same time its application is much more practical compared to other methods. However, rather than obtaining a transcriptome-wide profile, methylation points in candidate RNAs can be tested. As a weakness, the false-positive rate is high, and throughput is low.

1.1. m^6A modification in apoptosis

Following the discovery and functional characterization of m^6A regulatory proteins, studies focused on the biological roles of m^6A modifications. Many studies have reported that they play a role in various functions such as cell differentiation, biological clock regulation, and response to cellular stress (L. He et al. 2019). In addition, m^6A has been reported in disease progression and its suppressive or inducing roles have been observed in many types of cancer, such as lung cancer, breast cancer and cervical cancer (L. He et al. 2019; S. Liu et al. 2020). However, these studies focused on the functions of m^6A regulator proteins rather than the genome-wide methylation profile. The effects of m^6A regulator genes (METTL3, FTO and IGF2BP1) on various cancer cells have been studied and their roles in apoptosis have been mentioned.

Vu et al. demonstrated that depletion of METTL3 in human acute myeloid leukemia cells decreases the methylation level and increases p-AKT activation and apoptosis by reducing translation of MYC, BCL2 and PTEN (Vu et al. 2017). In another study, METTL3 knockdown in breast cancer cells reduces proliferation and accelerates apoptosis via Bcl-2, that is highly translated due to methylation, acts as the target of METTL3, which promotes tumor inhibition (H. Wang, Xu, and Shi 2020). Lin et al. showed that METTL3 increases the expression of pro-survival Bcl-2 and downregulates the pro-apoptosis regulator Bax as well as inactive caspase-3 resulting in reduction of apoptosis in gastric cancer cell (Sen Lin et al. 2019). Also, METTL3 can similarly regulate apoptosis in lung cancer (Wei, Huo, and Shi 2019). Besides the suppressive effect of METTL3 in apoptosis, triggering effects were shown in some studies. Song et al. found that METTL3 promotes cell apoptosis via TFEB-signaling pathway in cardiomyocytes (Song et al. 2019).

The role of m^{6}A methylation in apoptosis is not limited to methyltransferases. Some demethylase and reader proteins have also been studied. Huang et al. reported FTO promotes proliferation and suppresses the apoptosis of human acute myeloid leukemia cells (Y. Huang et al. 2019).

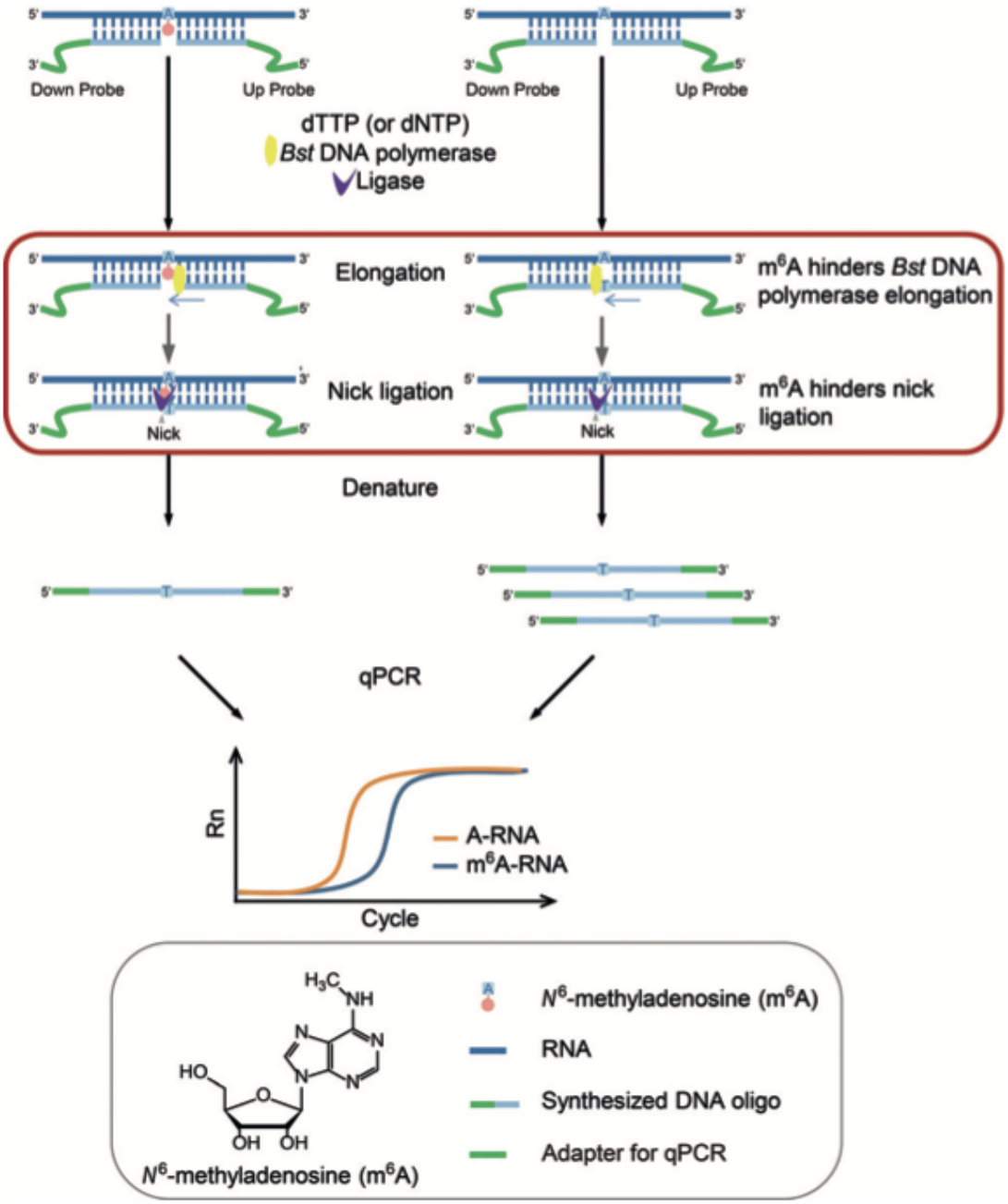

Figure 1.8. Schematic representation of SELECT experiment (Xiao et al. 2018).

It was shown that FTO inhibits proliferation and invasion and increases apoptosis by demethylation of MZF1 providing stability (J. Liu et al. 2018). IGF2BP1 enhances DDIT3 expression, which inhibits cell proliferation as well as promotion of apoptosis in human hepatocellular carcinoma cells (F. Xu et al. 2019).

The relationship of m^6A regulatory proteins with apoptosis was determined physiologically or with respect to the fate of target RNA, depending on the methylation, without specifically identifying apoptotic pathways. All of these studies show that m^6A modifications may play role in apoptosis. However, genome-wide m^6A RNA modifications can also be regulated by other methyltransferases or demethyltransferase (METTL14, WTAP, RBM15B and KIAA1429, ALKBH5). The contribution of other potential methylation enzymes is unclear and the profile of genome wide m^6A is not known. Additionally, intrinsic or extrinsic pathway specific m^6A methylation profiles have not been reported genome wide yet.

1.2. Aim

This study aims to obtain the m^6A methylated RNA transcriptome of HeLa cells in which the extrinsic apoptotic pathways is induced by TNF-alpha.

CHAPTER 2

MATERIALS and METHODS

2.1. Cell culture, drug treatment and transfection

HeLa cells were obtained from DSMZ GmbH (Gibco) and cultured in RPMI 1640 (with L-Glutamine, Gibco) medium containing 10% fetal bovine serum (FBS) (Gibco) and 1% penicillin-streptomycin (Gibco) at 37°C and 5% CO_2.

1x 10^6 HeLa cells were seeded on 10 cm dish (Sarstedt) and incubated overnight for TNF-alpha (Merck Millipore) treatment. Previous studies (TUBITAK Project 113Z371) showed that 75 ng/ml TNF-alpha with 10 µg/ml cycloheximide (CHX) (Applichem) for 24h is sufficient to reach LD_{50} in HeLa cells (Miura, Friedlander, and Yuan 1995). 1.2x 10^6 ME180 cells were seeded and treated with 10 µg/ml CHX and 30 ng/ml TNF-alpha for 24h. In addition, 5 µg/ml CHX and 10 ng/ml TNF-alpha were optimized for 1.2x 10^6 MCF7 cells. CHX was used as a negative control to obtain minimum cytotoxic effect. All experiments were conducted with three replicates. *P* values were calculated with student's t-test.

HeLa cells were transfected with si-METTL3 (Dharmacon) to be used in RNA/protein isolation followed by western blotting and SELECT experiments. Before using si-METTL3 and off target siRNA (Dharmacon) as a negative control, 100 µM siRNA solution was prepared in 1x siRNA buffer [60 mM KCl (Sigma), 6 mM HEPES-pH 7.5 (Gibco), and 0.2 mM $MgCl_2$ (Applichem)]. All stock solutions were aliquoted and stored at -20 °C.

Transfection was performed by seeding 0.6 x 10^6 cells on 10 cm dish (Sarstedt) and growing overnight. siRNA (Tube 1) and DharmaFECT transfection reagent (Tube 2) were diluted in separate tubes. In tube 1, 800 µl of the siRNA in serum-free RPMI 1640 (with L-Glutamine, Gibco) was prepared by adding 2 µl of 100 µM siRNA to 798 µl of serum-free medium to obtain 25 nM siRNA concentration. In tube 2, 800 µl of diluted

DharmaFECT transfection reagent in serum-free RPMI 1640 (with L-Glutamine, Gibco) was prepared by using 4 µl transfection reagent. After both tubes were incubated for 5 minutes at room temperature, the contents of tube 1 was added to tube 2 to obtain a total volume of 1600 µl. The mixture was incubated for 20 minutes at room temperature, and then 6400 µl antibiotic-free RPMI 1640 (with L-Glutamine, Gibco) with FBS was added to the mixture. By that time, culture medium was with 8000 µl fresh medium. Then, cells were incubated at 37°C in 5% CO_2 for 72 hours.

To treat the transfected cells with TNF-alpha, firstly, $0.6x10^6$ cells were seeded on 10-cm dishes (Sastedt) and incubated overnight. Transfection protocol was performed as described above. 37.5 ng/ml TNF-alpha with 2.5 µg/ml CHX was applied to siRNA transfected cells at the 56^{th} hour of transfection. TNF-alpha/CHX treated cells transfected with off-target siRNA were used as control groups.

2.2. Apoptosis measurement

Drug-treated cells were analyzed by flow cytometry (FACSCANTO, BD) to measure apoptosis rate by Annexin V-FITC and 7AAD-PerCP (BD), labelling. Firstly, cells were harvested by using Trypsin-EDTA (Gibco, 0.25%) and washed with 1x PBS. Culture media and PBS were saved to recover death cells. After cell pellets were dissolved with 50 µl of annexin binding buffer (BD), 10 µl of Annexin V-FITC and 10 µl of 7AAD-PerCP were mixed and incubated for 15 minutes at room temperature in the dark. Before the analysis of samples, stained cell mixtures were diluted by adding 200 µl 1x PBS (Gibco). As a control group, (1) cells with 50 µl of annexin binding buffer and no dyes, (2) cells with 50 µl of annexin binding buffer (BD) and only 10 µl of Annexin V, (3) cells with 50 µl of annexin binding buffer (BD) and only 10 µl of 7AAD were used for flow cytometry analysis. Cells having negative staining for both dyes were accepted as live. Annexin V positive/ 7AAD negative cell population represent early apoptotic stage, whereas Annexin V negative/ 7AAD positive cell was considered as death. Lastly, late apoptotic cells were regarded as Annexin V negative/ 7AAD positive.

2.3. Total RNA isolation and DNase treatment

Transfected and drug-treated cells were harvested with Trypsin-EDTA (Gibco, 0.25%) and washed with 1x PBS. After the complete removal of 1x PBS, cell pellets were suspended in 1 ml TRIzol™ reagent (Invitrogen). The protocol from manufacturer was followed to isolate RNA as described below. Cell lysate in TRIzol™ (Invitrogen), was incubated for 5 minutes at room temperature to dissociate nucleoprotein complexes. Then, 0.2 ml chloroform (Sigma) was added and mixed by shaking followed by incubation for 2 minutes. The sample was centrifugated for 15 minutes at 12.000× g at 4°C to separate it into aqueous, interphase and organic phases. Aqueous phase containing RNAs was carefully transferred to a new tube without any part of other phases. 0.5 ml of 100% RNase free isopropanol (Sigma) was added to the aqueous phase and incubated for 10 minutes at 4°C. It was followed by centrifugation at 12.000× g at 4°C for 10 minutes. The white gel-like pellet was resuspended and washed with 75% ice-cold ethanol. After centrifugation for 5 minutes at 7500× g at 4°C, RNA pellet was air-dried completely for 5 minutes. 20 µl of DNase and RNase free water (Gibco) was used to dissolve the pellet and kept -80°C until use.

The concentrations of isolated RNA were measured by NanoDrop Spectrophotometer (Thermo Fisher Scientific). Quality control of RNAs was examined by 260/280 and 260/230 absorbance ratios, which should be ~2, and %1 agarose gel electrophoresis in TBE (Tris-borate-EDTA buffer, 890mM Tris-borate, 890mM boric acid, 20mM EDTA.) for 25 min at 100 V. Gel image was obtained from UV light via AlphaImager (Model IS-2200, AlphaImager High Performance Gel Documentation and Image Analysis System).

50 µg total RNA was used for DNase treatment. 2.5 µl of 10X TURBO™ DNase buffer and 3 µl TURBO™ DNase (Thermo Fisher Scientific) was added to the RNA sample in a 25 µl reaction. Then, the reaction mixture was incubated at 37°C for 30 minutes. DNase activity was blocked by adding 2.5 µl of 10X DNase Inactivation Reagent (Thermo Fisher Scientific). Incubation of mixture for 5 minutes at room temperature was followed with centrifugation 12.000× g at 4 room temperature for 90 seconds, and then supernatant was transfered into a new tube. Quantity and quality control of DNase treated total RNA was determined as described above.

2.4. cDNA synthesis and quantitative PCR

Complementary DNA synthesis was performed by using Thermo Scientific RevertAid First Strand cDNA Synthesis Kit (Thermo Fisher Scientific). 1 µg of total RNA was combined with the following reagents in the indicated order: 1 µl Random Hexamer primer, 4 µl of 5X Reaction Buffer, 1 µl of RiboLock RNase Inhibitor, 2 µl of 10 mM dNTP mix and 1 µl of RevertAid M-MuLV RT. After centrifugation briefly, the reaction mixture was incubated for 5 minutes at 25°C, then for 60 minutes at 42°C following 70°C incubation for 5 minutes to terminate the reaction. 180 µl of nuclease free water was then added into 20 µl of cDNA mixture to obtain 5ng/µl concentration and stored at -80 °C.

qPCR reaction was prepared by combining 6.25 µl of GoTaq® qPCR Master Mix (Promega), 4.25 µl of nuclease-free water, 1 µl of 5 µM forward and reverse primer mix and 1 µl of cDNA. Standard two-step PCR amplification was applied by Rotor-Gene Q 2plex Platform (Qiagen). The mix was incubated at 95°C for 2 minutes as initial denaturation, 45 cycles of denaturation at 95°C for 15 seconds and annealing at 60°C for 1 minute following a melting step. For normalization, GAPDH was used as a housekeeping gene. All qPCR reactions were performed with 2 technical and 3 biological replicates for each sample.

2.5. m^6A individual-nucleotide-resolution cross-linking and immunoprecipitation (miCLIP)

Three replicates of TNF-alpha-treated cells, and CHX-treated negative controls were sent to Eclipse Bioinnovations (San Diego) for immunoprecipitation with Eclipse m^6A validated antibody, library preparation and high-throughput sequencing on NovaSeq machine. Sequencing was performed as SR75 on the HiSeq 4000 platform.

Table 2.1. The list of primer sequences used in this study

Genes	Forward 5'-3'	Reverse 5'-3'
METTL3	AGATGGGGTAGAAAGCCTCCT	TGGTCAGCATAGGTTACAAGAGT
METTL14	GAGTGTGTTTACGAAAATGGGGT	CCGTCTGTGCTACGCTTCA
WTAP	TTGTAATGCGACTAGCAACCAA	GCTGGGTCTACCATTGTTGATCT
RBM15	AAGATGGCGGCGTGCGGTTCCGCTGTG	AAGTTCACAAAGGCTACCCGCTCATCC
FTO	CTTCACCAAGGAGACTGCTATTTC	CAAGGTTCCTGTTGAGCACTCTG
ALKBH5	TCCAGTTCAAGCCTATTCG	CATCTAATCTTGTCTTCCTGAG
YTHDF1	TAAGGAAATCCAATGGACGG	TTTGAGCCCTACCTTACTGGA
YTHDF2	CCTTAGGTGGAGCCATGATTG	TCTGTGCTACCCAACTTCAGT
YTHDF3	TGACAACAAACCGGTTACCA	TGTTTCTATTTCTCTCCCTACGC
YTHDC1	TCAGGAGTTCGCCGAGATGTGT	AGGATGGTGTGGAGGTTGTTCC
YTHDC2	GTGTCTGGACCCCATCCTTA	CCCATCACTTCGTGCTTTTT
IGF2BP1	TAGTACCAAGAGACCAGACCC	GATTTCTGCCCGTTGTTGTC
IGF2BP2	ATCGTCAGAATTATCGGGCA	GCGTTTGGTCTCATTCTGTC
IGF2BP3	AGACACCTGATGAGAATGACC	GTTTCCTGAGCCTTTACTTCC
PRRC2A	AGGGCAAGTCCTTAGAGATCC	TTCAGGCTTGGAAGGTTGGC
FMR1	CAGGGCTGAAGAGAAGATGG	ACAGGAGGTGGGAATCTGA
HNRNPA2B1	AGCTTTGAAACCACAGAAGAA	TTGATCTTTTGCTTGCAGGA
HNRNPC	TAAGGAAATCCAATGGACGG	TTTGAGCCCTACCTTACTGGA
HNRNPG	TAAGGAAATCCAATGGACGG	TTTGAGCCCTACCTTACTGGA
PHLDA1	CTTCACTGTGGTGATGGCAGAG	CCTGACGATTCTTGTACTGCACC
IFI6	CTCGCTGATGAGCTGGTCT	ATACTTGTGGGTGGCGTAGC
PAWR	GCCGCAGAGTGCTTAGATGAG	GCAGATAGGAACTGCCTGGATC
HRK	GACTTGTGGATGGTGGAGGG	ACCAGATAGCAGGGCTCTCA
GADD45B	CCTGCAAATCCACTTCACGC	GTGTGAGGGTTCGTGACCAG
GAPDH	ACT CCT CCA CCT TTG ACG C	GCTGTAGCCAAATTCGTTGTC
Pri-SELECT	ATGCAGCGACTCAGCCTCTG	TAGCCAGTACCGTAGTGCGTG

2.6. Bioinformatic analysis

Differentially methylated RNAs on TNF-alpha treated HeLa cells were identified by Eclipse Bioinnovations (San Diego). All reads were mapped to the human genome UCSC version GRCh38/hg38. The clusters identified in the IP sample were normalized against a paired input sample. A peak was defined as a cluster with $\log_2$ fold enrichment ≥ 3 and p-value ≤ 0.001. The $\log_2$ fold change referred to the fold enrichment in eCLIP versus the paired input determined by Yates' Chi-square Test or Fisher's Exact Test. The data was provided including chromosome number, start and end point of methylation, log2 Fold Change values, gene names and Ensembl gene IDs with their respective features.

The pie chart depicted the relative frequency of peaks that map to each feature type, with a peak log2 fold enrichment ≥ 3 and p-value ≤ 0.001. Metagene plots depicted the average number of peaks mapped to certain genomic regions. The number of peaks was calculated for each region of every gene. The lengths of the regions were then normalized, and the average number of peaks for a set number of positions along the regions were calculated.

With differentially methylated 632 RNAs, pathway enrichment was carried out by using Gene Ontology database. All differentially methylated apoptotic genes were classified based on their expression level, fold change and location of methylation. Candidate genes were confirmed by using (1) the normalized file of clusters with chromosome, start position, stop position, and (2) crosslinking file which listing coordinates of antibody binding sites, to ensure the presence of a DRACH motif at the crosslinking site.

2.7. Validation of m^6A-methylated genes by SELECT

SELECT assay was used to validate m^6A methylation on candidate genes following the protocol described by (Xiao et al. 2018) 1.5 µg total RNA was mixed with 1 µl of 40 nM up oligomer, 1 µl of 40 nM down oligomer and 1 µl of 5 µM dTTP in 17

µl 1× CutSmart buffer (50 mM KAc, 20 mM Tris-HAc, 10 mM MgAc2, 100 µg/ml BSA, pH 7.9 @ 25°C) (New England Biolabs). Before the addition of enzymes, RNA and oligomer mixture were incubated at a temperature gradient in TurboCycler 2 thermal cycler (Blue-Ray Biotech): 90°C for 1 min, 80°C for 1min, 70°C for 1 min, 60°C for 1 min, 50°C for 1 min, and then 40°C for 6 min to anneal. The enzyme mixture was then prepared by adding 0.01 U Bst 2.0 DNA polymerase (New England Biolabs), 0.5 U SplintR ligase (New England Biolabs) and 10 nmol ATP (New England Biolabs). 3 µl of enzyme mixture was add to a final volume of 20 µl. The final reaction mixture was incubated for 20 min at 40°C and denatured for 20 min at 80°C. Subsequently, qPCR was performed in Rotor-Gene Q 2plex Platform (Qiagen). 10 µl of GoTaq® qPCR master mix (Promega), 1 µl of 200 nM forward and reverse SELECT primer mix and 2 µl of the final reaction mixture were mixed and run at the following condition: 95°C, 5min; (95°C, 10s; 60°C, 15s; 60°C, 1min; 95°C, 15s (collect fluorescence at a ramping rate of 0.05°C/s); 4°C, hold. As a loading control B-actin was used.

2.8. Protein extraction and western blotting

TNF-alpha treated or si-METTL3 transfected HeLa cells were harvested and washed with 1x PBS. Subsequently, the cell pellet was dissolved with 2 µl of the protease inhibitor cocktail (100X) (CST) and 48 µl of radio immunoprecipitation assay (RIPA) solution, which contains 25 mM Tris•HCl pH 7.6, 150 mM NaCl, 1% NP-40, 1% sodium deoxycholate, 0.1% SDS (CST) a ratio of 1:100. After vortexing for 1 minute, it was kept on ice for 10 minutes and this process was repeated 4 times to facilitate lysis. The sample was centrifuged at 12.000 × g for 15 minutes to remove the cell debris. Supernatant was transferred into a new tube and protein concentration was determined with Bradford assay. The protein sample diluted 1: 3 was mixed with 200 µl of Bradford solution and the absorbance value was measured at 495. The concentrations were determined according to the optimized absorbance-concentration graph. The extracted protein was stored at -20°C.

Western blotting was performed according to Mahmood and Yang 2012. 10% separating gel (40% acrylamide mix, separating buffer pH 8.8, APS and TEMED), and

5% stacking gel (40% acrylamide mix, stacking buffer pH 6.8, APS and TEMED) were prepared. 20 µg of protein was loaded into each well. Protein ladder (New England Biolabs) was used to estimate protein size. Electrophoresis was run at 80 V for 4 hours to separate proteins according to their size. Then, proteins on gel were transferred onto a PVDF (Thermo Scientific) membrane by using wet-transfer method and run at 30 V overnight. Following the transfer, the membrane was blocked with 5% non-fat dry milk (CST-E) prepared with 1x Tris Buffered Saline (TBS) and 1% Tween 20 (FISHER) for 1 hour at room temperature. The membrane was washed with TBS-T solution for 3 times in 30 minutes. Primary rabbit antibody (CST) incubation for METTL3, METTL14, RBM15 and FTO on the membrane was carried out overnight at 4°C. It was followed by TBS-T washing and anti-rabbit IgG-HRP conjugate secondary antibody (CST) incubation for 1 hour at room temperature. After one more round of TBS-T washing, membranes were treated with chemiluminescent substrate (ThermoFisher) solution for 1 minutes and the membrane was scanned by BIO-RAD, VERSADOC 4000 MP. Anti-B actin (CST) was used as a loading control.

2.9. Polysome fractionation assay

Polysome profiling was performed to assess the sedimentation of translated mRNAs on a sucrose gradient according to the number of bound ribosomes. First, HeLa cells were lysed and loaded on top of a 5-70% sucrose gradient. The gradient was centrifuged at 27.000 RPM and 40Cfor 2.55 hours. After ultracentrifugation, the gradient was fractionated by monitoring at A254. The fractions were collected and pooled as untranslated mRNAs (top fractions), monosomal fractions, light polysomes and heavy polysome-associated mRNAs (bottom fractions). The collected fractions were extracted by using acid phenol-chloroform extraction method. The translational status of mRNA populations is analyzed by Q-PCR amplification and its relative quantification in each fraction.

Table 2.2. The list of oligomer sequences used in SELECT experiment

Genes	SELECT Oligomers
MALAT1-A2511-UP	5'-tagccagtaccgtagtgcgtgAATTACTTCCGTTACGAAAGTCCT-3'
MALAT1-A2511-DOWN	5phos/CCTCAGGATTTAAAAAATAATCTTAACTCAAcagaggctgagtcgctgcat-3'
MALAT-m^{6}A2515-UP	5'-tagccagtaccgtagtgcgtgAATTACTTCCGTTACGAAAG-3'
MALAT-m^{6}A2515-DOWN	5phos/CCTTCACATTTTTCAAACTAAGCTACTcagaggctgagtcgctgcat-3'
PHLDA1-UP	5'-tagccagtaccgtagtgcgtgCGCAAGTTTTCAGTAGGGTGATG-3'
PHLDA1-DOWN	5phos/CCAAACTACTTGATCTGGTGcagaggctgagtcgctgcat-3'
PAWR-UP	5'tagccagtaccgtagtgcgtgGATCTTTCTATAGTAAAAG-3'
PAWR-DOWN	5phos/TTGTAGATATTTTTTGcagaggctgagtcgctgcat-3'
IFI6-UP	5'tagccagtaccgtagtgcgtgGGAGAGTGATAGACAAAG-3'
IFI6-DOWN	5phos/TCTGGATTCTGGcagaggctgagtcgctgcat-3'
GAPDH-UP	5'tagccagtaccgtagtgcgtgTCCACTTTACCAGAG-3'
GAPDH-DOWN	5phos/TAAAAGCAGCCCTcagaggctgagtcgctgcat-3'
B-actin-UP	5'tagccagtaccgtagtgcgtgCCCCGTCACCGGAG-3'
B-actin-DOWN	5phos/CCATCACGATGCcagtcagaggctgagtcgctgcat-3'

CHAPTER 3

RESULTS

3.1. TNF-alpha-induced apoptosis in HeLa cells

To induce the extrinsic apoptotic pathway, HeLa cells were treated with 75ng/ml TNF-alpha and 10 μg/ml CHX because TNF-alpha is functional only in the presence of CHX in HeLa cells (Miura et al. 1995). CHX treated cells were used as a negative control. TNF-alpha reduced viability from 83.6% to 53% while inducing the rate of early apoptosis from 10.2 % to 35.1% (Figure 3.1, $P< 0.05$)

Total RNA was isolated from TNF-alpha/CHX-treated HeLa cells. Based on 260/230 and 260/280 ratios of 2.00 and agarose gel analysis, the purity of total RNAs was defined to be of sufficient quality. Turbo DNase treatment was performed to eliminate trace amount of DNA as visualized on a 1% agarose gel. No degradation was observed in the total RNA (Figure 3.2).

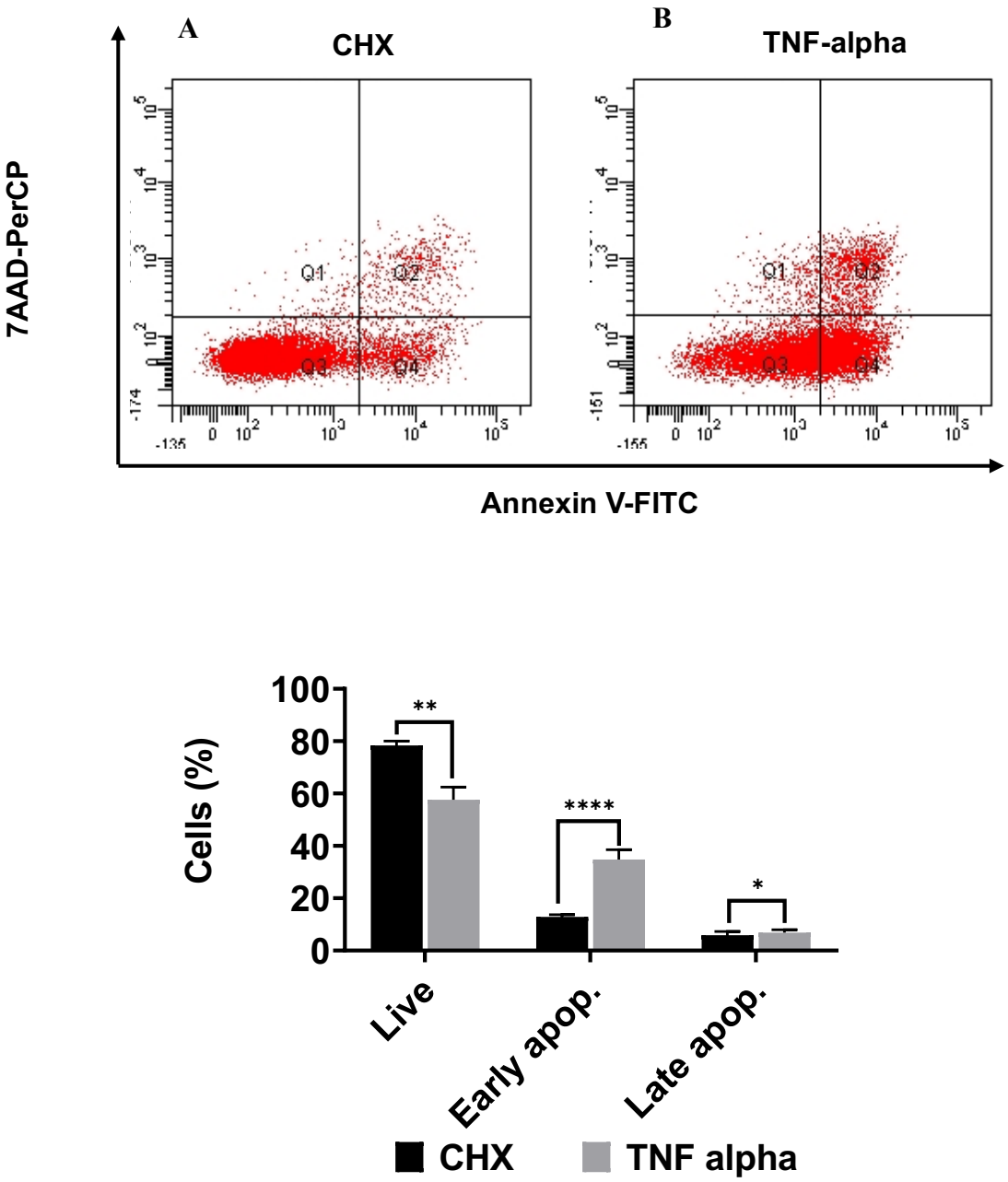

Figure 3.1. **A-B.** Representative FACS profiles of TNF-alpha-treated cells. Apoptosis rate was determined by flow cytometry using AnnV-FITC/7AAD-PerCP. Q1 (AnnV-/7AAD+) represents dead cells; Q2 (AnnV+/7AAD+) is late-stage apoptotic cells; Q3 (AnnV-/7AAD-) belongs to viable cells and Q4 (AnnV+/7AAD-) is early-stage apoptotic cells. **C.** Apoptosis rate of TNF-alpha-induced HeLa cells. Histograms represent mean ± SD of three independent experiments. Statistical analyses were carried out using student's t-test (**** $P < 0.0001$; ** $P < 0.01$; *$P < 0.05$).

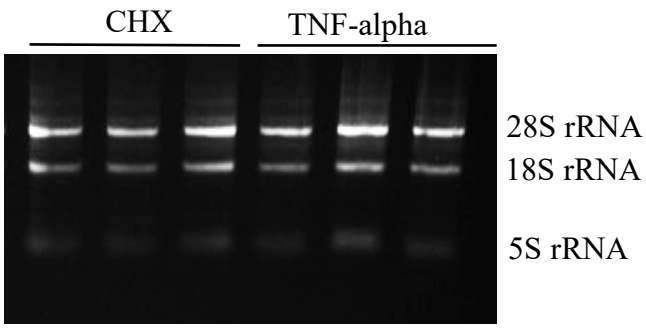

Figure 3.2. Total RNAs isolated from CHX and TNF-alpha treated HeLa cells.

3.2. Gene expression level of m^{6}A regulators

Gene expression analysis of writer and eraser proteins under TNF-alpha-treated conditions were examined by quantitative PCR and western blotting. WTAP was induced by 2.76-fold ($P<0.001$) compared to control group. ALKBH5 was downregulated by 1.25-fold ($P<0.05$). However, there was no remarkable increase in METTL3, METTL14, RBM15 and FTO (Figure 3.3). TNF-alpha treatment led to a significant decrease in the protein level of RBM15 by 3.03-fold ($P<0.05$) and METTL3 by 2.38-fold ($P<0.05$) (Figure 3.4).

The transcript amount of m^{6}A reader genes were determined by qPCR. Although there was no significant change in mRNA levels of m^{6}A reader proteins, YTDHC1, YTHDC2, PRRC2A, FMR1, HNRNPA1B2 and HNRNPG were upregulated almost 1.5-fold whereas IGF2BP2 was downregulated by 1.5-fold (Figure 3.5).

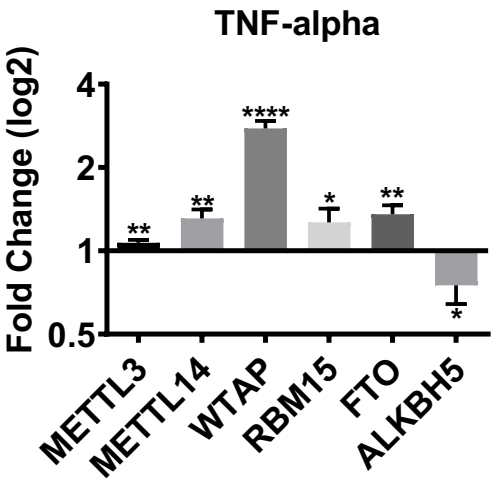

Figure 3.3. Gene expression level of m^{6}A regulators. Transcript levels were quantified relative to reference gene GAPDH by ΔΔCq method. Log2 fold change in response to TNF-alpha treatment. Results for each gene are expressed as mean ± S.D. of three experiments performed in triplicates. Student's unpaired t-test was used to calculate p-values (P<0.05(*). P<0.01 (**), P<0.0001 (****).

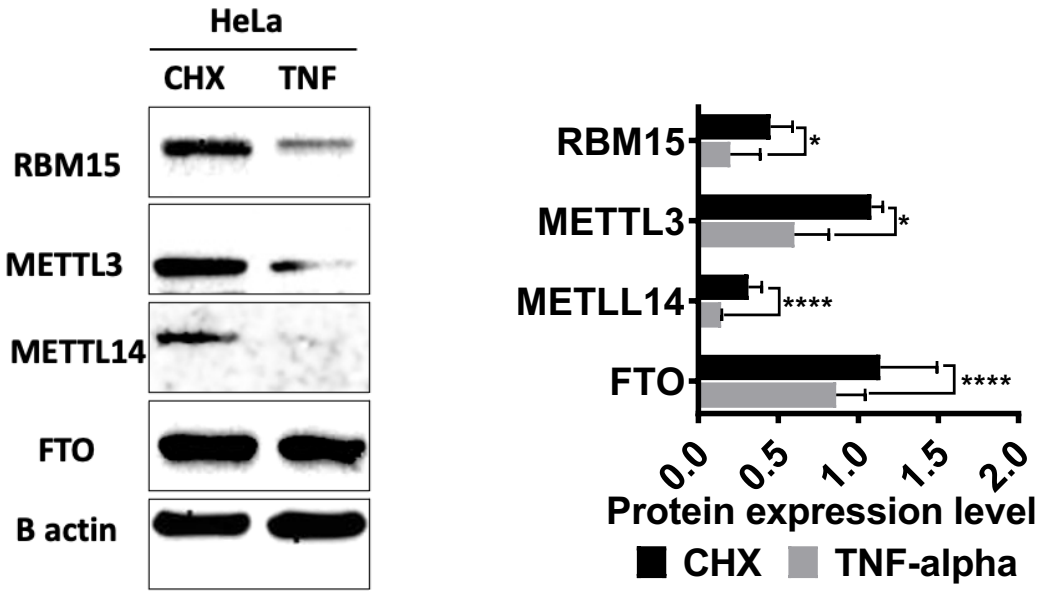

Figure 3.4. Western blot analysis for RBM15, METTL3, METTL14 and FTO in TNF-alpha-treated cells (n=3).

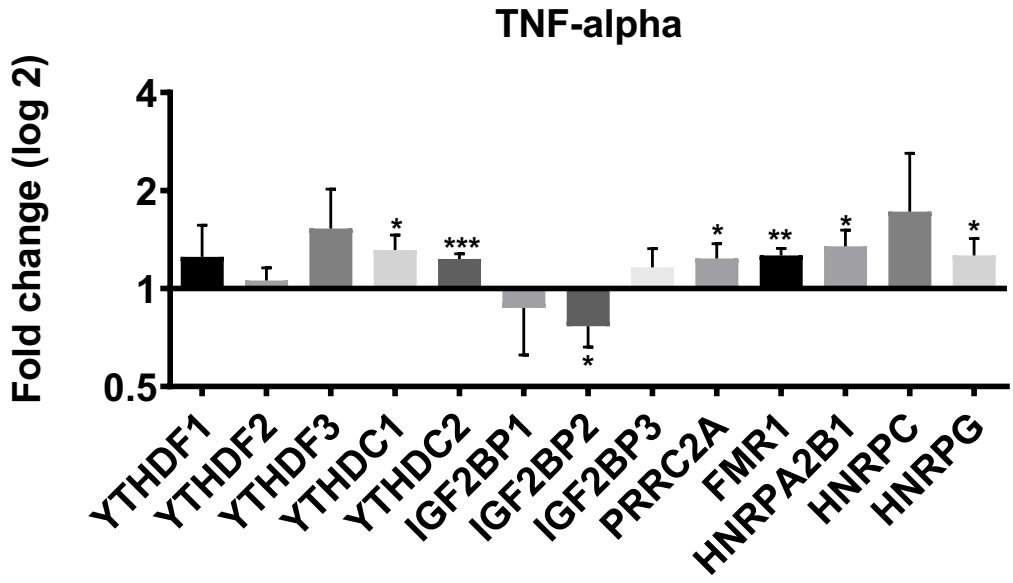

Figure 3.5. m^{6}A reader mRNA expression levels in TNF-alpha treatment (n=3). The error bars represent standard deviations of the means and statistical analysis was performed by using student's unpaired t-test (P<0.05(*). P<0.01 (**), P<0.001 (***).

3.3. Genome wide m^{6}A profile by miCLIP and bioinformatic analyses

To determine genome wide m^{6}A methylation profile under TNF-alpha treatment, m^{6}A sites in transcripts were determined using miCLIP. Metaintron plot of miCLIP showed that m^{6}A is enriched at 3 ′ UTR in TNF-alpha treatment while it is found at some level throughout the transcriptome. When the distribution of differentially methylated sites on transcriptome was examined in TNF-alpha, a similar pattern was seen. However, the average peak values were higher in genes with enhanced m^{6}A level than in reduced m^{6}A methylated genes (Figure 3.6). Besides, there was motif heterogeneity for decreased m^{6}A methylated genes while a majority of sites fall into a GGAC context in increased m^{6}A methylation at 44,71% (Figure 3.7).

The metaintron peaks at CDS were lower than at 3'UTR. When the number of enhanced methylated genes was examined as a percentage distribution, there were 43.25% methylation CDS with 1272 methylation points. However, 999 methylation points at 3'UTR make up 33.97% of the total. Although similar percentages (CDS 54.10% and 3'UTR 32.02%) were observed in genes whose methylation decreases with TNF-

alpha, the number of methylation points was lower than the genes with increased methylation. While the decreasing point of 534 methylation level in CDS was detected, this number was 316 in 3'UTR (Figure 3.8).

miCLIP results showed that methylation levels are increased at 2941 positions whereas 987 methylation sites are reduced. All differential m^{6}A modifications was distributed throughout 632 genes. Pathway enrichment analysis for positively and negatively differentially m^{6}A methylated 632 genes was performed by using Gene Ontology (GO) databases. 30 most significant pathways and the corresponding numbers of m^{6}A methylated genes in these pathways are shown in Figure 3.9. Also, apoptosis related pathways from biological processes were determined. 99 out of 632 genes with differential methylation levels were found to be involved in apoptotic pathways (Figure 3.10).

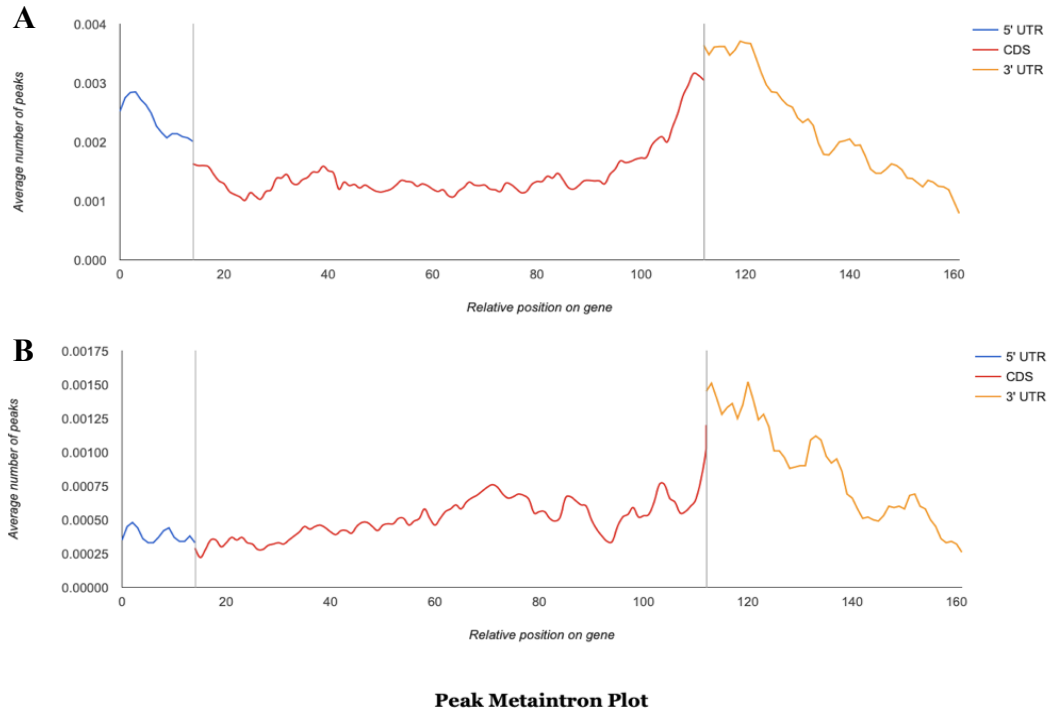

Figure 3.6. Distribution of m^{6}A in metaintron profile of miCLIP for (A) enriched m^{6}A level and (B) reduced m^{6}A level in TNF-alpha treatment. Metaintron are produced by averaging signals from input normalized miCLIP.

Figure 3.7. Motif analysis of m^{6}A methylated genes by HOMER.

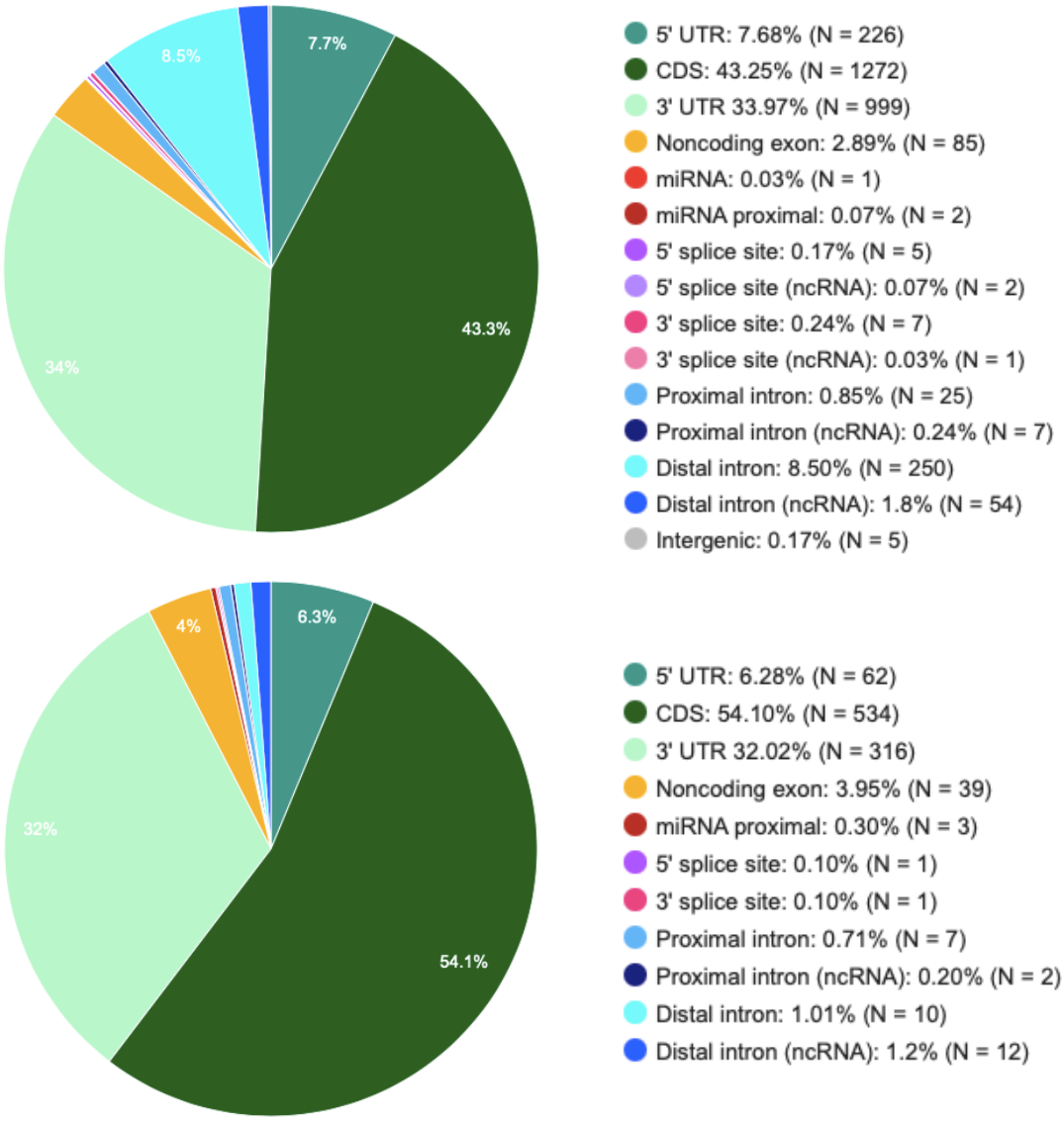

Figure 3.8. Pie chart depicting percentage of mRNA m^{6}A clusters in each non overlapping transcript segment for enriched m^{6}A level (upper part) and reduced m^{6}A level (lower part).

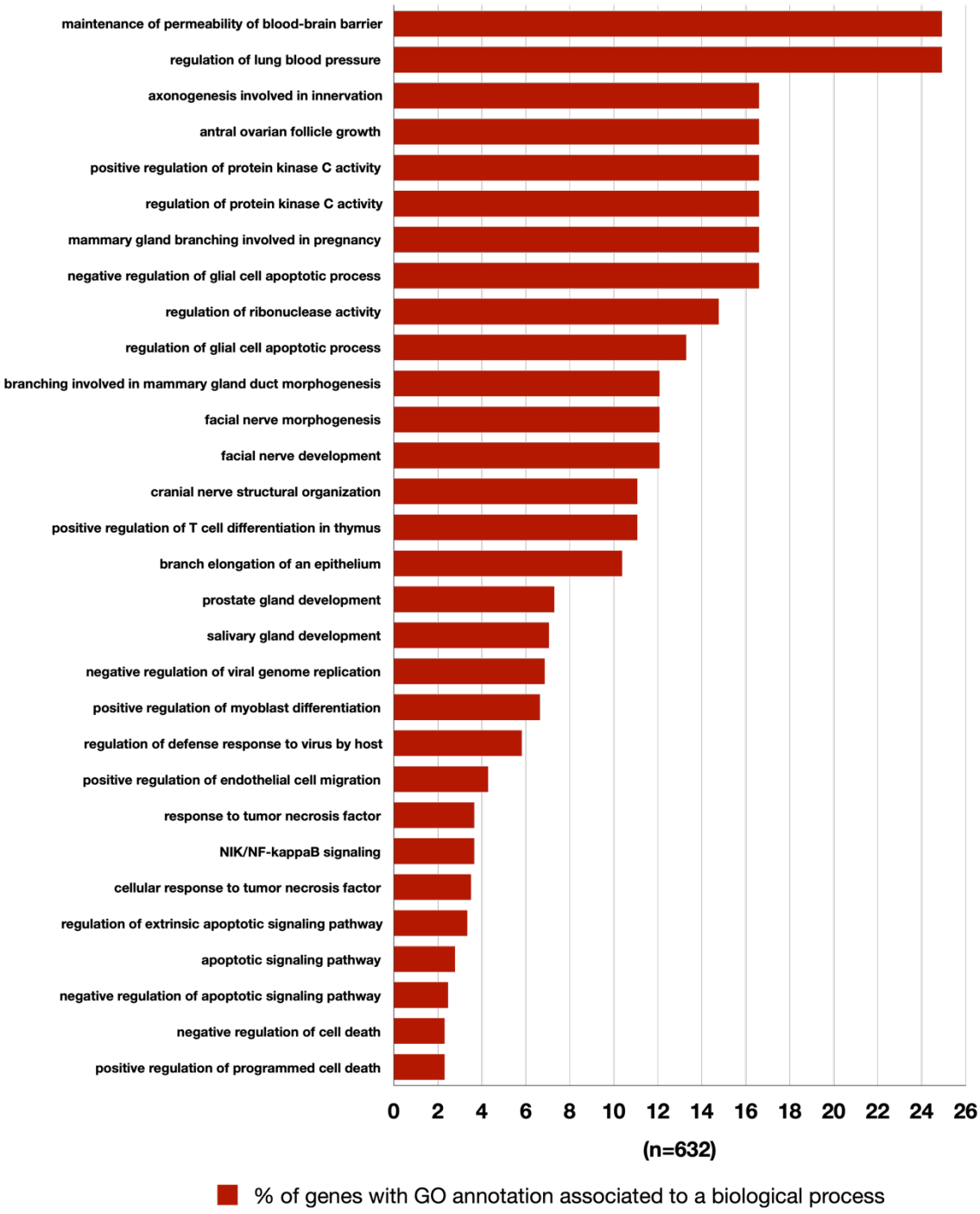

Figure 3.9. GO enrichment analysis. Bar graphs show gene number included in each biological process. Results are shown only for P value match of < 1e-15.

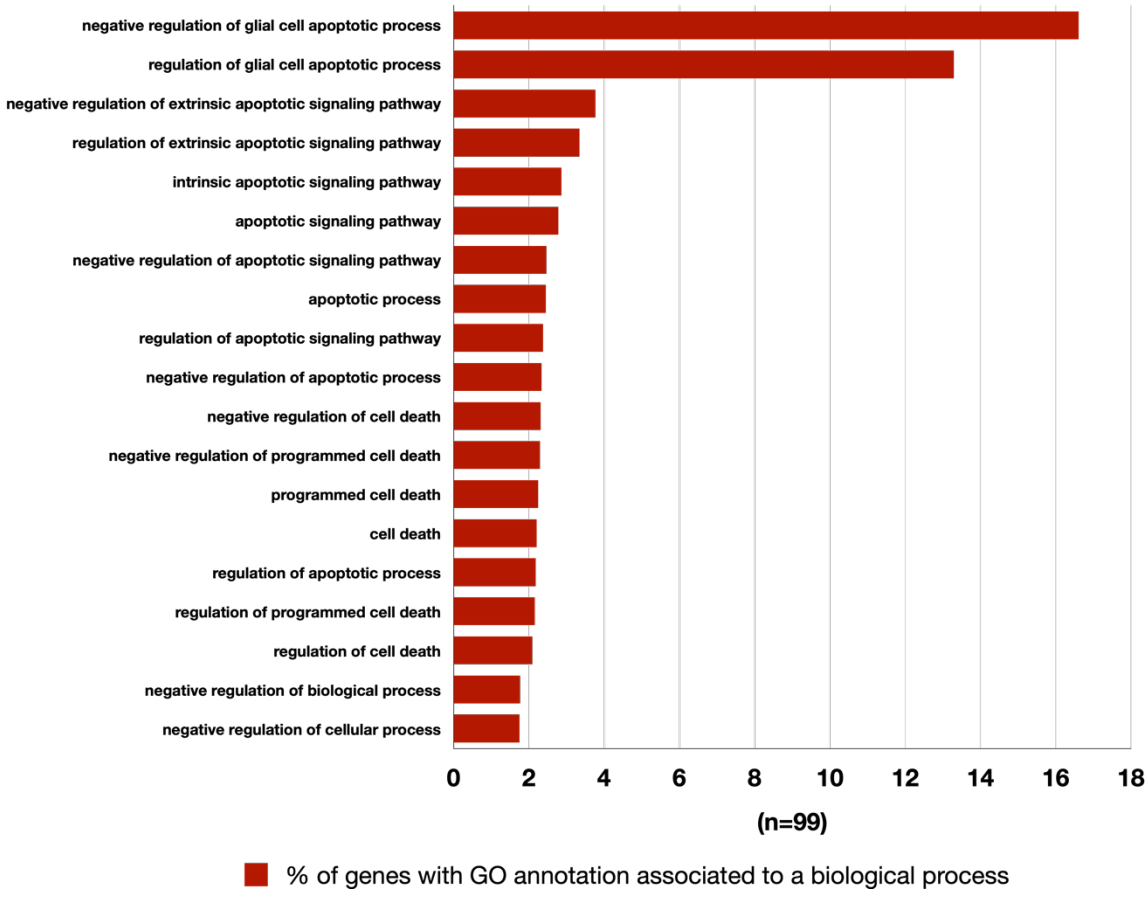

Figure 3.10. GO analysis including apoptotic pathway for differentially m^{6}A methylated genes.

99 apoptotic genes were further analyzed based on their methylation fold change, cellular expression level, methylation site and apoptotic role to select candidate genes. The methylation sites of the candidate genes were first verified in IGV. In the miCLIP method, since false positive data might be seen due to various reasons such as antibody cross reactivity with different methylation etc., it should be ensured that the candidates meet the following criteria: (1) observation of RNA precipitated by m^{6}A antibody, (2) observation of m^{6}A antibody binding site on RNA and (3) occurrence of these two conditions on DRACH motif in IGV. Five genes meeting all three conditions were determined as candidates (Figure 3.11), which are Pleckstrin Homology Like Domain Family A Member 1 (PHLDA1), Pro-Apoptotic WT1 Regulator (PAWR), Interferon Alpha Inducible Protein 6 (IFI6), Growth Arrest and DNA Damage Inducible Beta (GADD45B) and Harakiri, BCL2 Interacting Protein (HRK).

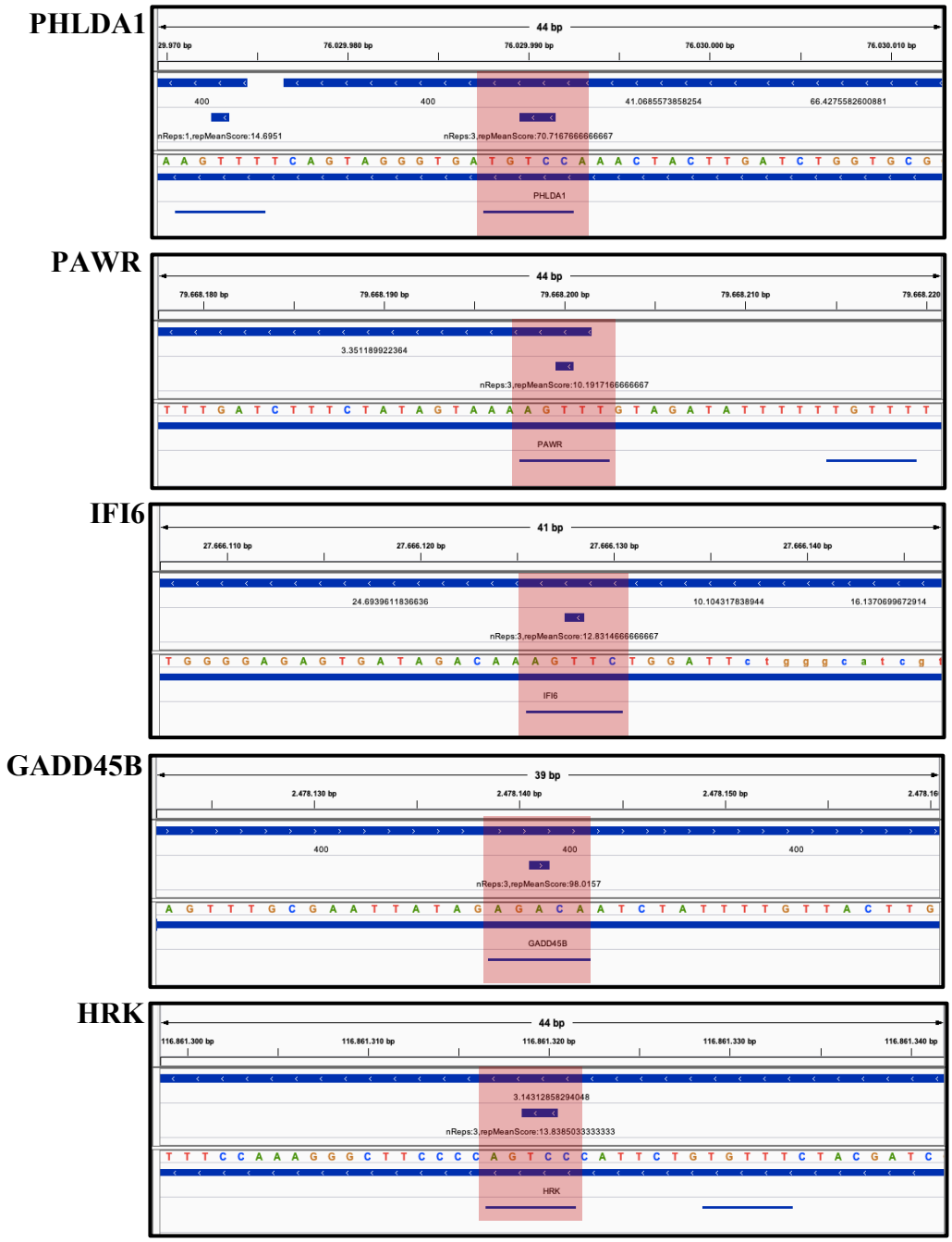

Figure 3.11. IGV screenshots of m^{6}A sites based on m^{6}A antibody crosslinking site and precipitated RNA. The regions where the three factors intersect are shown in a red box.

Table 3.1. The list of candidate genes and their m^{6}A enrichments and sites

Candidates	Fold change (log 2)	Site
PHLDA1	4.35	3' UTR
IFI6	3.06	3'UTR
PAWR	3.30	Distal intron
HRK	3.06	3'UTR
GADD45B	3.78	3' UTR

3.4. Validation of candidates by SELECT

The SELECT method was used to validate m^{6}A methylations in candidate mRNAs, as it is cheap, fast and base specific. In this method, DOWN and UP oligomers flanking the m^{6}A sites are ligated by Bst 2.0 polymers and SplintR ligase. The presence of a m^{6}A residue affects the ligation efficiency of oligomers negatively. The amount of ligated products is then quantified by qPCR(Figure 3.12).

First of all, MALAT-A2511 (negative) and MALAT1-m^{6}A2515 (positive) control groups (Xiao et al. 2018) were tested under the METTL3 KD condition to test the accuracy of the method. Since METTL3 silencing causes a decrease in the amount of m^{6}A, the amount of product is expected to be higher than the negative control, and this is reflected in the qPCR as a lower Cq value.The efficiency of METTL3 knockdown was first examined by western blotting with the protein lysate collected 72 hours after si-METTL3 transfection (Figure 3.13). Since the MALAT1 negative region did not contain a m^{6}A residue, the amount of qPCR product was not affected by METTL3 KD and no Cq difference was observed between test and control groups. However, in the MALAT1 positive control, METTL3 silencing resulted in lower Cq as described above (Figure 3.14).

Following validation of the conditions SELECT method, the change in m^{6}A amounts under TNF-alpha treatment was tested by SELECT. In HeLa cells, an increase of 1.7 Cq for PHLDA1; 1,57 Cq for PAWR and 1.97 Cq for IFI6 was observed. Relatively

less amount of ligated product shows an increase in the amount of m^6A in direct proportion to miCLIP. Regions devoid of m^6A methylation DRACH motif on housekeeping gene, B-actin, was used as loading control. (Figure 3.15). SELECT results of TNF-alpha-treated ME180 showed a similar pattern with the TNF-alpha-treated HeLa cells. There are Cq differences of 0.69, 1.36 and 3.51 for PHLDA1, PAWR and IFI6, respectively. However, 1.08 cycle difference was observed for only PHLDA1 in TNF-alpha-treated MCF7 cells (Figure 3.15).

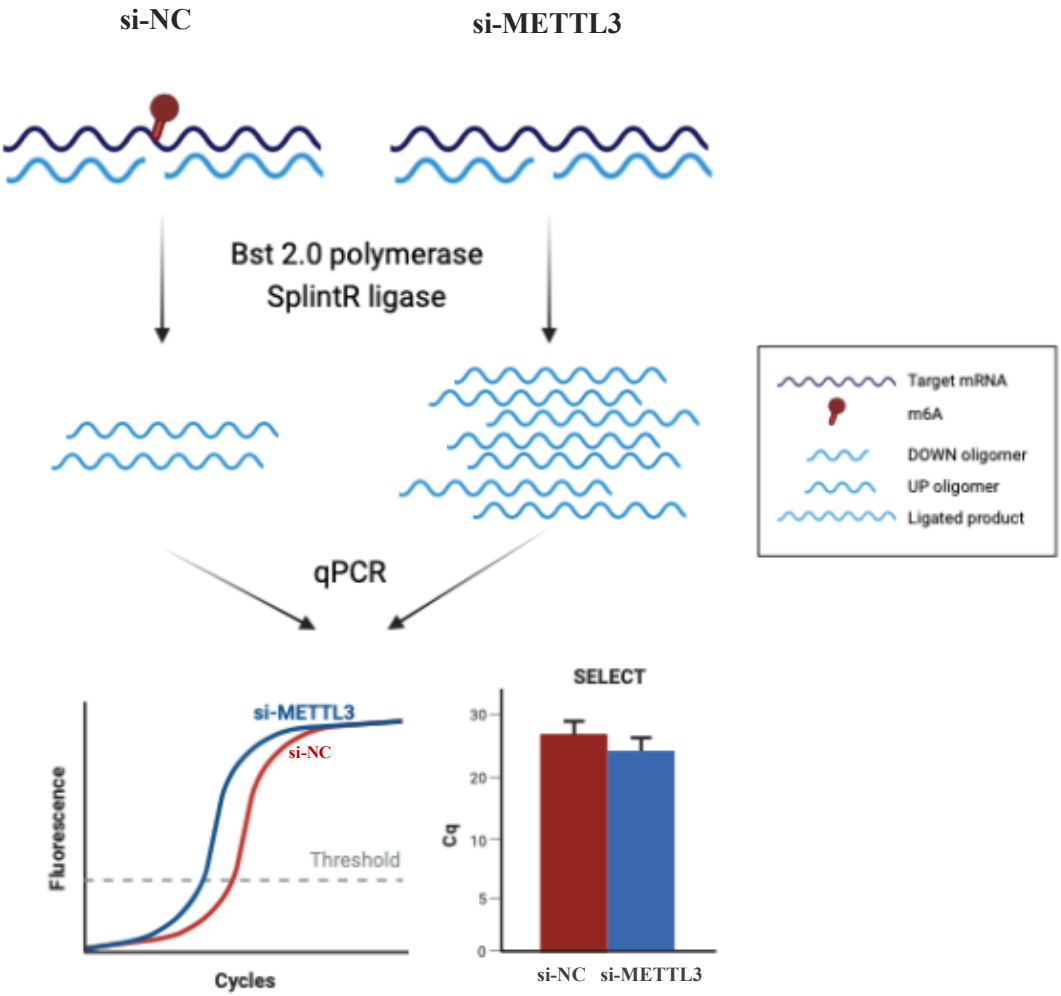

Figure 3.12. Schematic representation of SELECT procedure for m^6A validation.

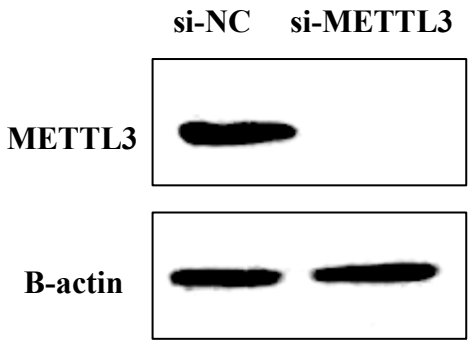

Figure 3.13. Western blot result for METTL3 KD. It was performed using 25µg of protein lysate collected 72 hours after siMETTL3 transfection.

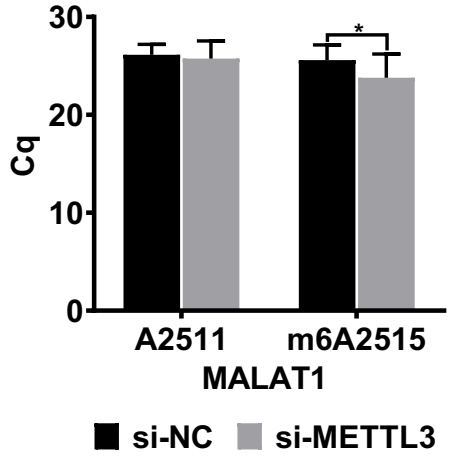

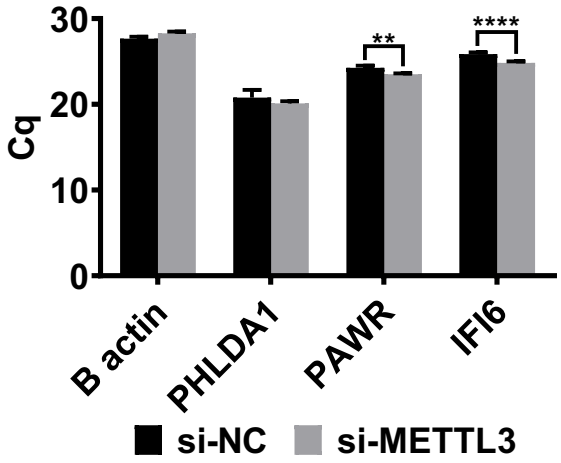

Figure 3.14. The threshold cycle (Cq) of qPCR showing SELECT results B-actin was used loading control. Bars represent mean ± SD for three biological replicates. Student's unpaired t-test was used to analyze. (P<0.0001 ****, P<0.01 **, P<0.05 *).

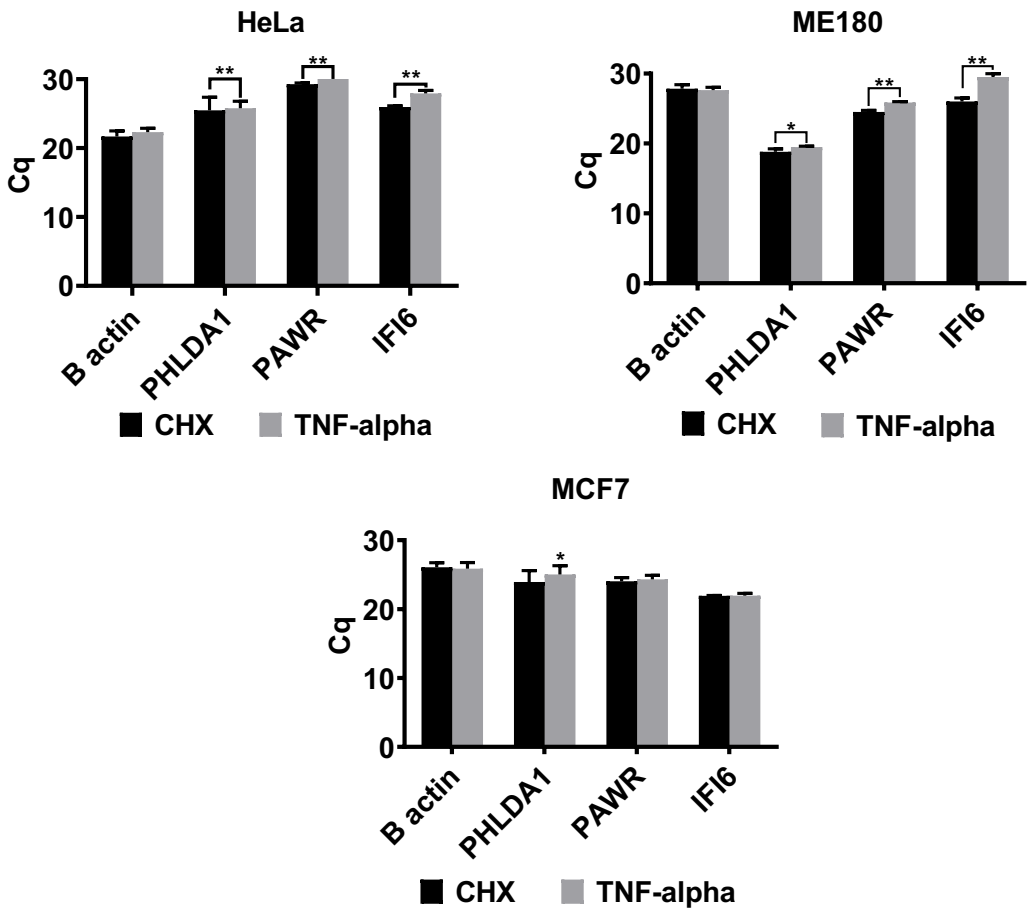

Figure 3.15. The Cq values of SELECT results for TNF-alpha treated HeLa, ME180 and MCF7 cells. Data are presented as mean ± SD; n= 3 for per group; Student's t unpaired test was applied (P<0.01 **, P<0.05 *). B-actin was used as a loading control.

3.5. Expression level of candidates

Gene expression levels in METTL3 KD and TNF-alpha-treated HeLa cells were analyzed by qPCR in order to gain insight into the fate of candidate genes. PHLDA1 was increased 1.5-fold in METTL3 KD and 3-fold in TNF-alpha treated cells. In contrast, PAWR was downregulated as 1.5-fold in METTL3 KD and 1.25-fold in TNF-alpha. However, there was no dramatic change in IFI6. Also, GADD45B and HRK were negatively affected by METTL3 silencing whereas no significant effect of TNF-alpha was seen (Figure 3. 16).

METTL3 KD HeLa cells were exposed to 37.5ng/ml TNF-alpha and 2.5 μg/ml CHX for 12h to induce the extrinsic apoptotic pathway. CHX treated (1) si-METTL3 or

(2) si-NC transfected and (3) TNF-alpha treated si-NC transfected HeLa cells were used as control groups. There was no significant difference in cell viability of METTL3 KD and negative control cells upon CHX treatment. METTL3 KD cells exposed to TNF-alpha displayed decreased viability from 75.5% to 50.4% while the percentage of early apoptotic cells rose from 18.2% to 42% (Figure 3.17, $P<0.05$). Relative expressions of candidate genes were also measured in response to METTL3 KD HeLa cells treated with CHX or TNF-alpha. PAWR did not show any significant differential expression. PHLDA1, IFI6, HRK and GADD45B were upregulated in CHX treated METTL3 KD HeLa cells by 1.95, 2.73, 2.08 and 1.27-fold, respectively. TNF-alpha treatment induced gene expression levels of PHLDA1 by 3.61-fold, IFI6 by 4.56-fold and HRK by 3.44-fold. GADD45B was not significantly affected in TNF-alpha treatment (Figure 3.18).

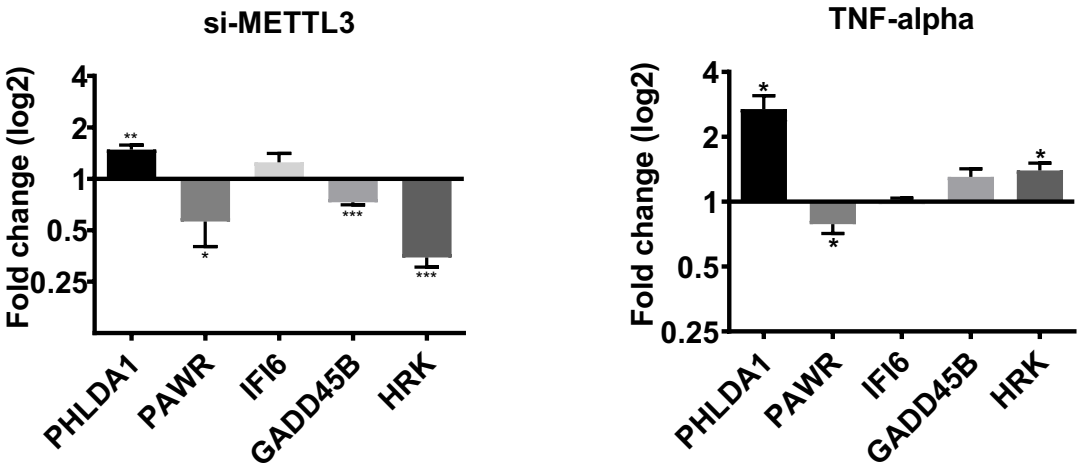

Figure 3.16. Expression levels of candidate genes in si-METTL3 (left) and TNF-alpha treatment (right) samples relative to the control and relative expression by qPCR. $P < 0.05$ is indicated as *, $P<0.01$(**) and $P < 0.001$ (***) based on student's unpaired t-test.

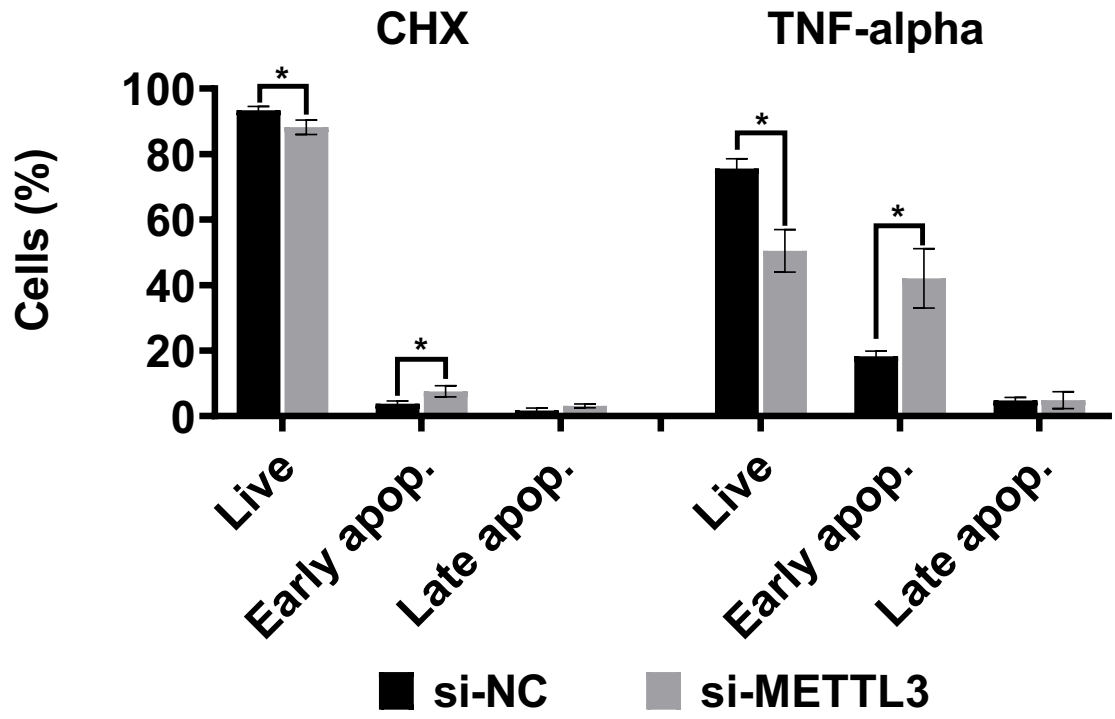

Figure 3.17. Cell viability of METTL3 KD HeLa cells treated with TNF-alpha. The rate of apoptosis was measured by flow cytometry. CHX treated si-NC and si-METTL3 were used as control groups. n=3, mean + SD, t-test was used for statistical analysis (P<0.05 *)

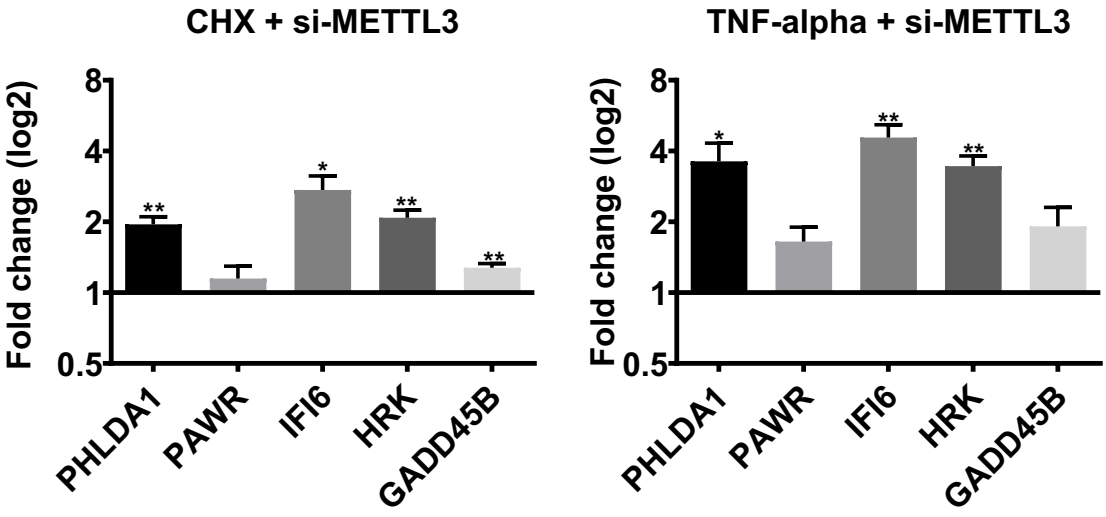

Figure 3.18. Relative gene expression levels of selected genes in METTL3 KD HeLa cells exposed to CHX (left) and TNF-alpha (right). Gene expression levels were quantified by qPCR. Bar represents means and SD of 3 biological replicates. Asterisks indicate statistical analysis for student's t-test (P<0.05 *, P<0.01**).

To analyze translational state of candidate genes, polysome profiling was performed with an experimental setup similar to that explained in Figure 3.17 in addition to METTL3 KD HeLa cells. The corresponding cell extracts were sedimented by centrifugation on 5-70% sucrose gradients. Fractions were pooled into 4 major fractions as mRNP, monosome, light polysome and heavy polysome based on A_{254} readings. METTL3 KD did not affect the global translation profile except for 80S. However, CHX causes translational inhibition. So, it negatively affected polysomal fractions in TNF-alpha treated HeLa cells (Figure 3.19). RT-qPCR analysis of total RNAs phenol-extracted from the polysomal fractions showed significantly decreased association of PAWR with the heavy polysome and GADD45B with the monosome fraction upon METTL3 KD, while IFI6 was upregulated in the mRNP fraction. However, specific changes were not seen in the polysome association of PHLDA1, IFI6, HRK and GADD45B (Figure 3.20). To analyze the polysome distribution of candidate genes in TNF-alpha treated METTL3 KD HeLa cells, qPCR was separately performed for CHX and TNF-alpha. Relative quantifications were calculated in accordance with si-NC transfected cells in both treatments. CHX reduced heavy polysome level in PHLDA1, PAWR, HRK and GADD45B by 5.1, 1.8, 2 and 2.7-fold, respectively. However, the polysome associations were increased by 2.6, 1.3, 36.4-fold for PHLDA1, PAWR and HRK in TNF-alpha treated METTL3 KD cells. GADD45B and IFI6 were decreased by 1.8- and 2.9-fold (Figure 3.21).

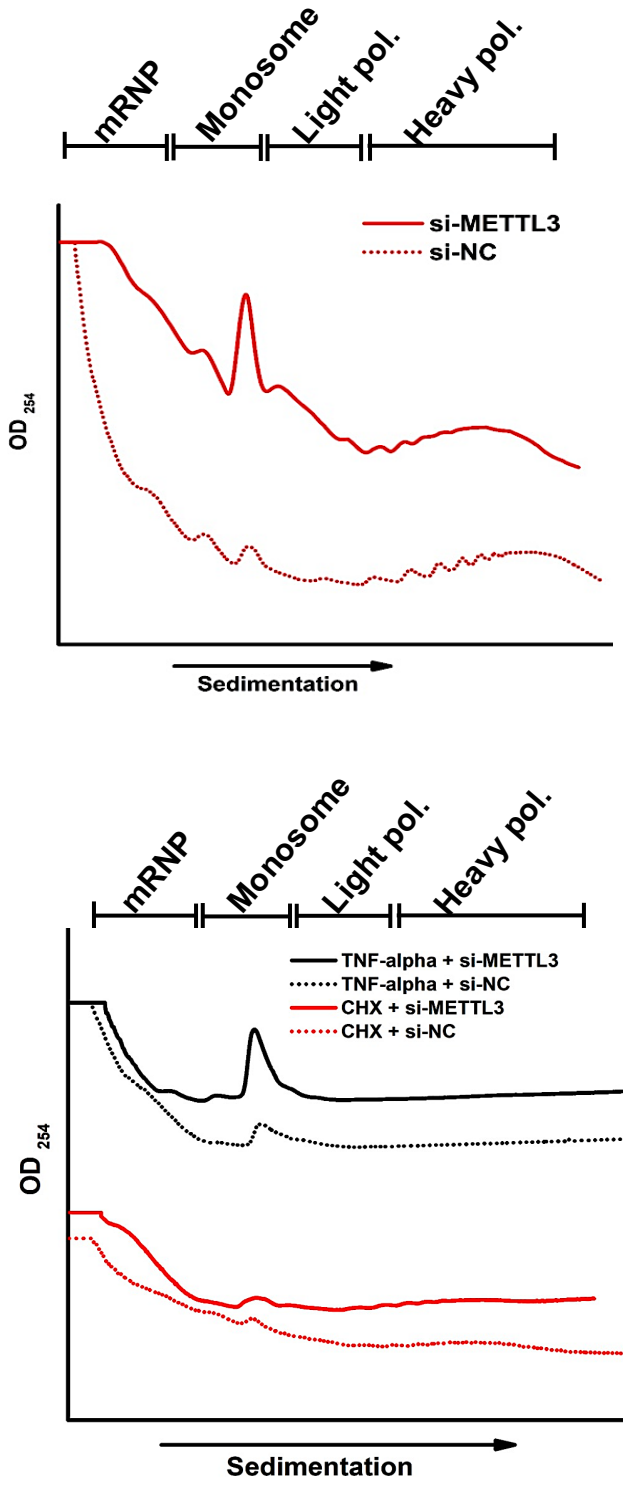

Figure 3.19. Polysome profile of si-METTL3 transfected HeLa cells without treatment (left), with CHX and TNF-alpha (right). Cell extracts were fractionated on 5%-70% sucrose gradients and fractions were collected using an ISCO sucrose density centrifugation system while reading absorbance at A_{254}. One of the representative experiments is shown here.

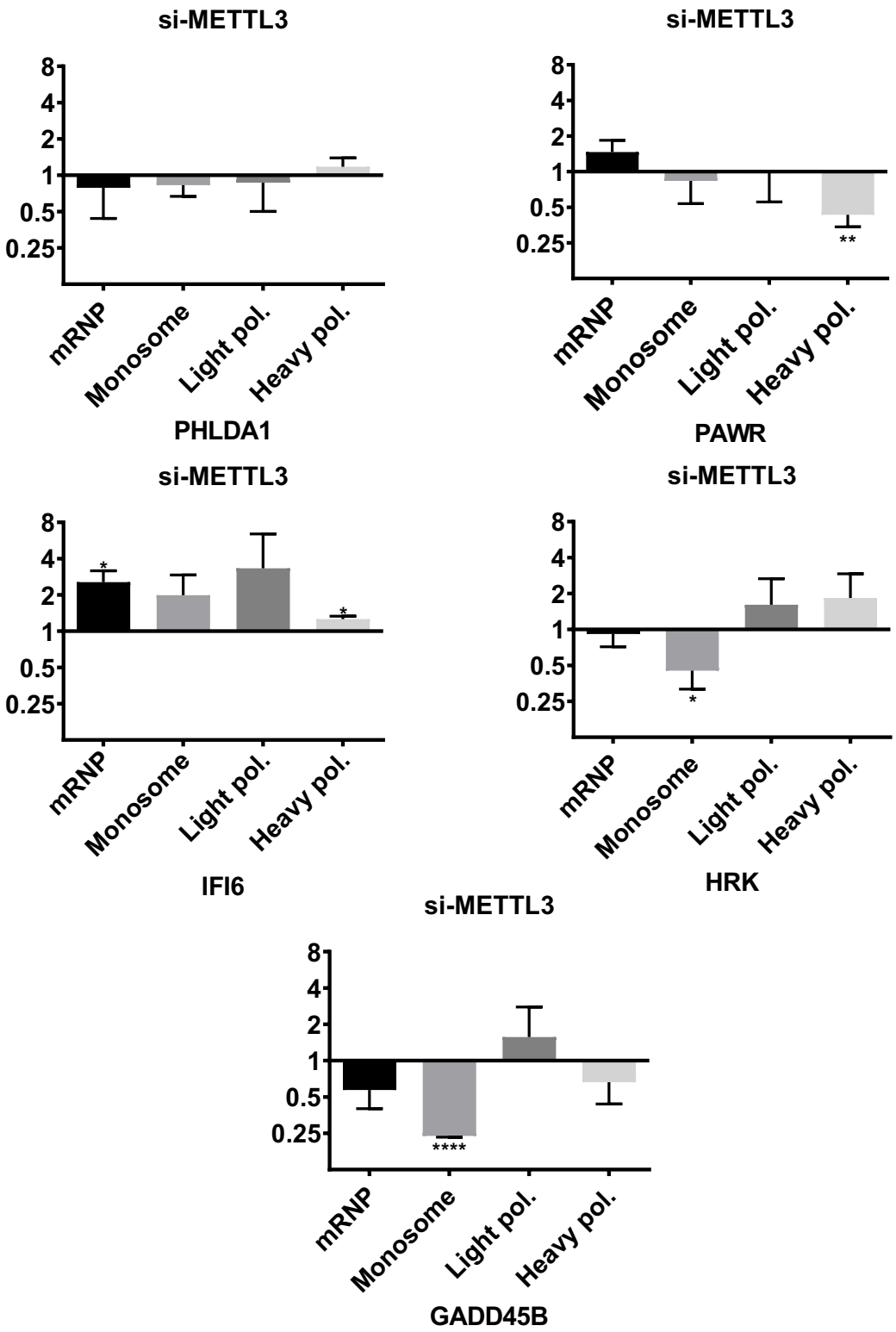

Figure 3.20. qPCR analyses of fractionated HeLa cells. qPCR analyses were performed with total RNAs isolated from fractionated HeLa cells transfected with si-METTL3. mRNP, monosome, light polysome and heavy polysome were pooled and the abundance of the PHLDA1, PAWR, IFI6, HRK AND GADD45B transcripts were quantified by qPCR. For each experiment, n = 3

biological replicates, bar represents the mean value. Data was analyzed by student's t-test (P<0.05*, P<0.01**, P<0.0001****).

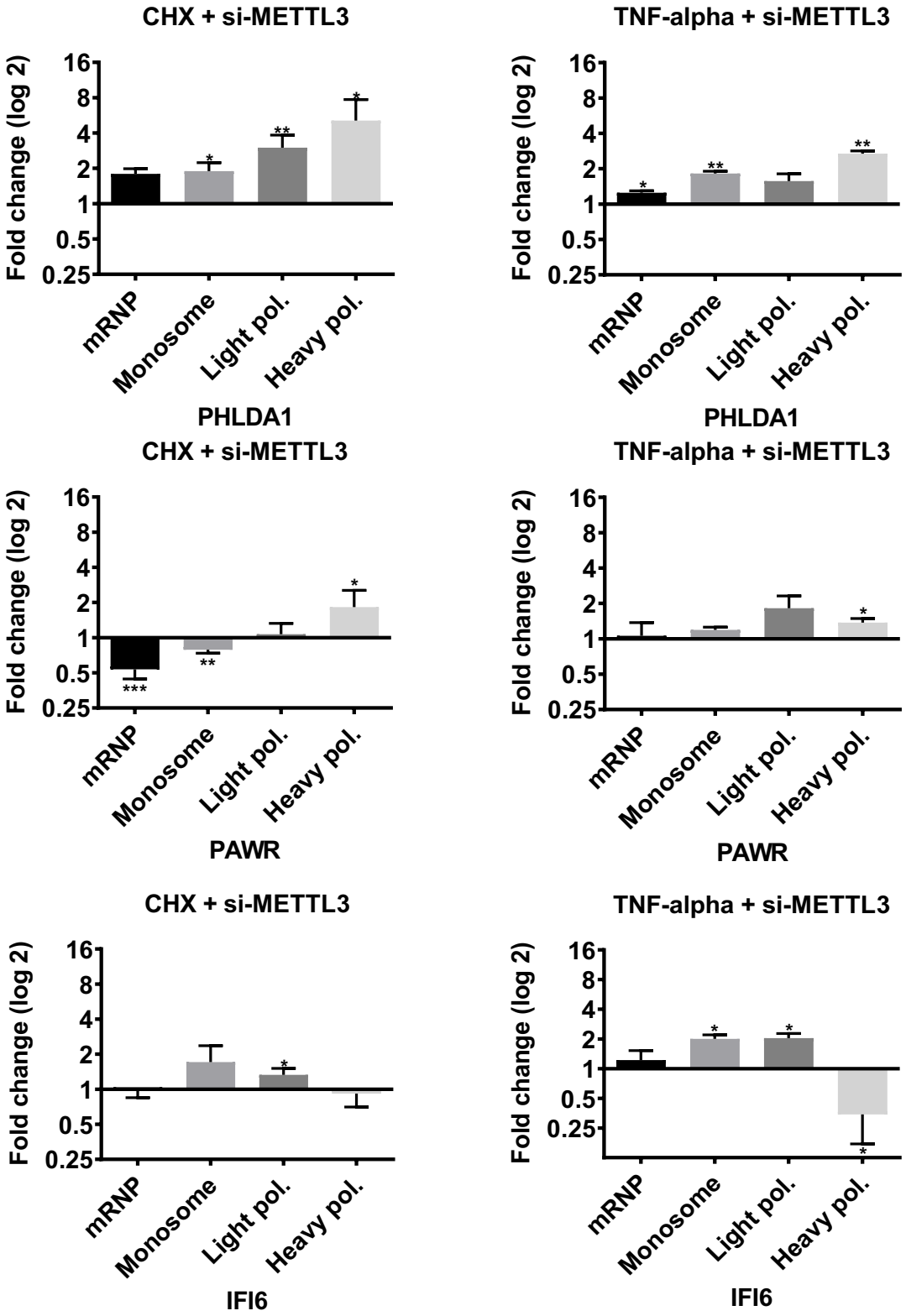

Figure 3.21. Steady-state mRNA levels of PHLDA1, PAWR, IFI6, HRK and GADD45B. Transcript amounts were measured by qPCR in METTL3 siRNA or control siRNA transfected cells treated with CHX (left) or TNF-alpha (right). Graphs

show mean + SD of qPCR replicates for one of three independent experiments with similar results. qPCR results normalized to GAPDH.

(Cont. on next page)

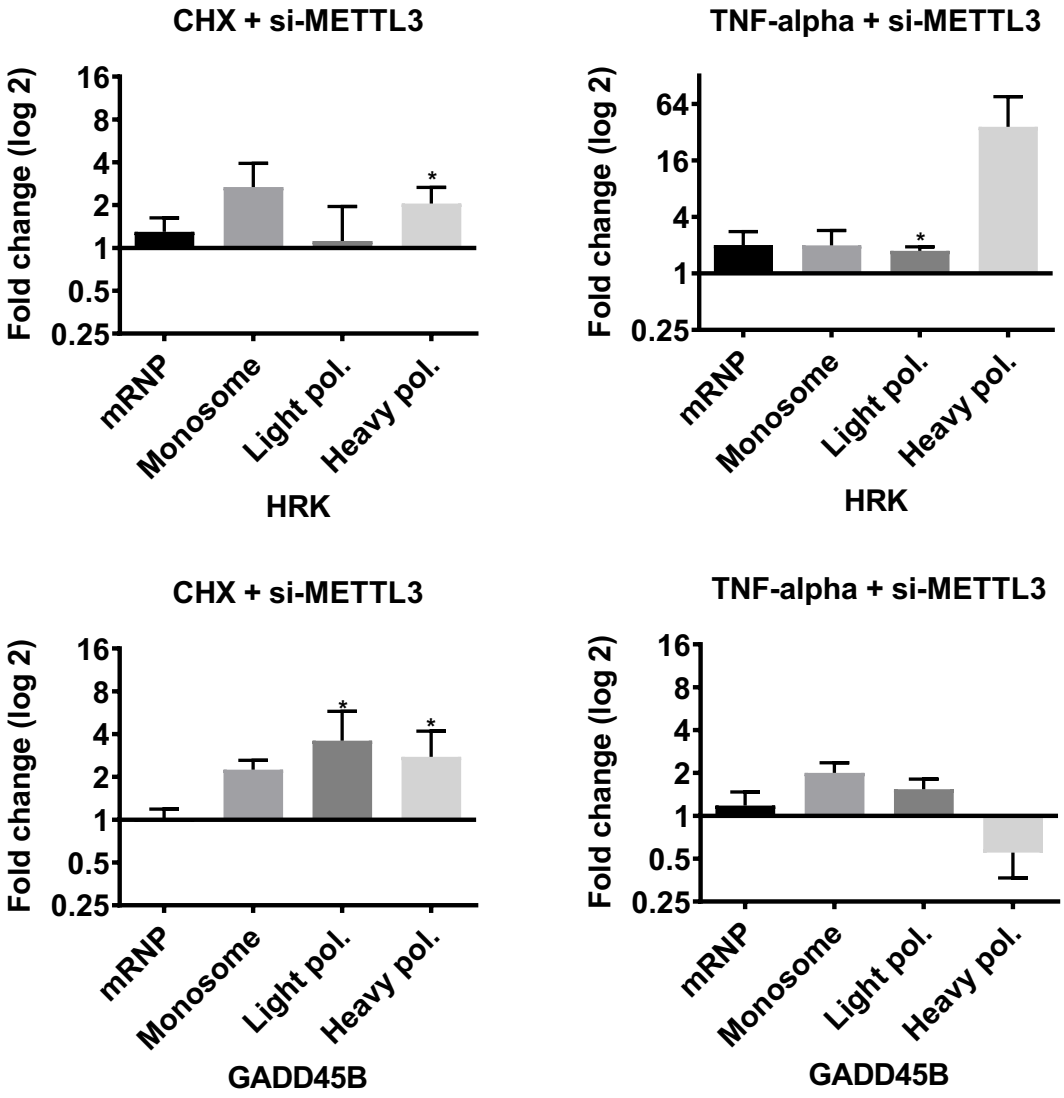

Figure 3.21. (cont.)

CHAPTER 4

DISCUSSION

Although there are many studies on the regulation of gene expression at the required time and in accordance with environmental conditions, these studies have focused on the epigenetic changes of DNA. Recent studies have focused on epitranscriptomics, showing the effect of biochemical RNA modifications on gene regulation and furthermore on the fate of mRNA. Studies in this relatively new field have aimed to identify m^6A methylation under various physiological and pathological conditions. There are limited number of studies covering m^6A methylation and apoptosis. The effect of RNA modifications on the regulation of apoptotic genes is intriguing. In light of all this information, it was hypothesized that m^6A RNA modifications are parts of co-transcriptional regulatory mechanisms in TNF-alpha induced apoptotic HeLa cells.

Firstly, gene expression level of writer and eraser proteins under TNF-alpha treatment was examined and qPCR result showed that there is not a dramatical change in expression except for WTAP (Figure 3.4). Interestingly, RBM15, METTL3 and METTL14 have reduced protein level in TNF-alpha treated cells (Figure 3.5). There is not always a linear correlation between RNA and protein level. Post-transcriptional modification of mRNA, miRNA action, protein half-life or protein damage may contribute to a high mRNA level without a corresponding protein level (Greenbaum et al. 2003). On the other hand, the transcript levels of the reader proteins did not show a statistically significant difference, remaining between 0.5-fold increase and decrease (Figure 3.6).

Based on the genome wide m^6A profile of TNF-alpha-treated HeLa cells, metaintron plot of miCLIP showed that 3'UTR region was affected to a greater extent compared to other regions (Figure 3.7.). The m^6A modifications found in the 3'UTR are widely associated with various aspects of mRNA metabolism and function, including altered splicing, decreased mRNA stability, altered mRNA stability and translation efficiency (Haussmann et al. 2016; Choe et al. 2018; Slobodin et al. 2017). In addition, the average peak number of genes with increased m^6A methylation is twice that of genes

with decreased methylation. Considering that the METTL3 protein level is decreased, the reason for the increase in the methylation level might be explained by the highly expressed WTAP, although it has no catalytic activity. WTAP can regulate m^6A methylation in its target genes via existing METTL3 (Ping et al. 2014; Schöller et al. 2018). Moreover, the consensus motif (GGAC) in differentially m^6A methylated genes, being close to 50%, may indicate the sequence targeted by WTAP. Ping et al. demonstrated that the motifs AGGACU (P = 1e-14) are enriched in WTAP binding clusters (Ping et al. 2014). Also, percentage of m^6A modifications is higher in CDS and 3'UTR (Figure3.9). While there is an increase in the methylation level in 2941 regions, the number of methylation regions that decrease is 987. However, 3,928 methylation sites correspond to 632 genes.

To analyze biological processes associated with 632 differentially methylated RNAs, gene ontology analysis was performed, and 30 important processes were identified (Figure 3.10). Furthermore, apoptosis related pathways were selected to identify differentially methylated apoptotic genes (Figure 3.11). 99 apoptotic genes having differential m^6A methylation were uncovered. PHLDA1, PAWR, IFI6, HRK and GADD45B were selected as candidates to look their fate as well as validation of their methylation. The pro-apoptotic role of PHLDA1 has been reported by overexpression or downregulation in many different studies (Janus et al. 2020, Adriana et al. 2018). In addition to induction of apoptosis, inhibition of cell proliferation causes cell death, but despite all this information, the pro-apoptotic mechanism of PHLDA1 is not fully known (Caf 2012). PAWR is a tumor suppressor protein that has been shown to induce apoptosis by suppressing BCL2 (Rah et al. 2015). IFI6 negatively affects apoptosis through the mitochondrial dependent pathway (Qi et al. 2015). HRK contributes to apoptosis regulation by interacting with the anti-apoptotic Bcl-xL and Bcl-2 (Kaya-Aksoy et al. 2019). Lastly, GADD45B is a pro-survival factor but it has been demonstrated that activation of GADD45B by NF-kB down-regulates pro-apoptotic JNK signaling induced by TNF receptors (De Smaele et al. 2001).

Before the validation of candidate genes, it was necessary optimize the SELECT procedure. Therefore, METTL3 KD cells were used with MALAT1-A2511 and MALAT1-m^6A2515, as a negative and positive control, respectively. MALAT1-A2511 did not show any significant Cq differences between METTL3 KD cells and its control cells, whereas lower Cq value was observed for MALAT1-m^6A2515 in METTL3 KD

cells (Figure 3.15). Lower Cq indicates a higher amount of ligated product of SELECT experiment. Ligation of UP and DOWN oligomers, which are specific to MALAT1 or any candidate genes, can be achieved in case of no or low level m^6A methylation, like METTL3 KD condition. As the next step, m^6A level of candidates were validated by SELECT in TNF-alpha-treated HeLa cells. The Cq values of PHLDA1, PAWR and IFI6 increased by 1.7, 1.57 and 1.97, respectively.

To investigate the fate of candidate genes, their expression levels were first examined in METTL3 KD and TNF-alpha treated HeLa cells. METTL3 KD negatively affected transcript level of candidates except PHLDA1. However, this might be caused by other m^6A methylation which are different from our candidates' position because METTL3 silencing affect total m^6A modification. In TNF-alpha treatment, PHLDA1 showed 3-fold enrichment while dramatic change cannot be observed for other candidates. Similar to METTL3 KD condition, expression level might be independent of specific m^6A methylation. METTL3 KD in CHX-treated HeLa cells resulted in an increase in the expression of PHLDA1, IFI6 and HRK by 1.95, 2.73, 2.08-fold. The relative expression levels of genes were 3.61, 4.56, 3.44-fold. To elucidate gene expression levels in METTL3 KD HeLa cells treated with TNF-alpha, we compared their expression levels, which exhibited a 2-fold increase in the expression of PHLDA1, IFI6 and HRK. These observations suggest a transcriptional effect of m^6A methylation in TNF-alpha-induced apoptosis. However, METTL3 KD causes less m^6A methylation in any site or RNA. Transcriptional changes could be caused by a global effect instead of target m^6A methylations of candidate genes. Therefore, m6A methylation level might be investigated by SELECT in METTL3 KD with TNF treatment. The differential expression had the same upregulation pattern for candidate genes, so we checked translational levels of genes by polysome fractionation assay. Our analyses showed no candidate genes being associated with the light or heavy polysomes in METTL3 KD HeLa cells. METTL3 KD HeLa cells treated with CHX resulted in the polysome association of PHLDA1, PAWR, HRK and GADD45B. However, TNF-alpha treatment decreased the association of PHLDA1, HRK, IFI6 and GADD45B.

CHAPTER 5

CONCLUSION

In this study, we identified and validated differentially expressed m^6A regulator genes and m^6A methylated RNAs in TNF-alpha induced apoptotic HeLa cells by qPCR, miCLIP and SELECT.

Despite the low level of METTL3, WTAP might cause raise of global m^6A methylation at 3'UTR. Around 50% of RNAs with increased m^6A methylation containing WTAP-specific motif supports this hypothesis. Although there was an increase in m^6A level in 2941 sites, m^6A residues decreased in 987 regions. All these methylation sites are located on a total of 632 genes. Of the 632 genes with a statistically significant difference in m^6A methylation, only 99 genes play a role in apoptosis. They were listed considering the methylation fold change, intracellular expression level and apoptotic role, and the data obtained from the miCLIP of the selected candidates were validated in IGV. The presence of DRACH motif of the m^6A antibody binding site on the immunoprecipitated RNA was accepted as IGV confirmation. Obtaining 0.29, 1.92 and 1.96 Cq differences in PHLDA1, PAWR and IFI6 in SELECT confirmed the increase in m^6A methylation in TNF-alpha treatment. Changes in the expression levels of candidates in METTL3 KD and TNF-alpha treated cells were not prominent. However, TNF-alpha treatment in METTL3 KD cells caused the differential expression of PHLDA1, IFI6 and HRK by almost 2-fold. Additionally, the polysome profiles of the candidate genes showed that METTL3 KD cells with TNF-alpha treatment probably affect the translational efficiency of the candidate genes as well.

REFERENCES

Anreiter, Ina, Quoseena Mir, Jared T. Simpson, Sarath C. Janga, and Matthias Soller. 2021. 'New Twists in Detecting MRNA Modification Dynamics'. *Trends in Biotechnology* 39 (1): 72–89. https://doi.org/10.1016/j.tibtech.2020.06.002.

Arya, R., T. Sarkissian, Y. Tan, and K. White. 2015. 'Neural Stem Cell Progeny Regulate Stem Cell Death in a Notch and Hox Dependent Manner'. *Cell Death and Differentiation* 22 (8): 1378–87. https://doi.org/10.1038/cdd.2014.235.

Berlivet, Soizik, Jérémy Scutenaire, Jean Marc Deragon, and Cécile Bousquet-Antonelli. 2019. 'Readers of the m 6 A Epitranscriptomic Code'. *Biochimica et Biophysica Acta - Gene Regulatory Mechanisms* 1862 (3): 329–42. https://doi.org/10.1016/j.bbagrm.2018.12.008.

Budhidarmo, Rhesa, and Catherine L. Day. 2015. 'IAPs: Modular Regulators of Cell Signalling'. *Seminars in Cell and Developmental Biology* 39: 80–90. https://doi.org/10.1016/j.semcdb.2014.12.002.

Caf, P. 2012. *Encyclopedia of Signaling Molecules*. *Encyclopedia of Signaling Molecules*. https://doi.org/10.1007/978-1-4419-0461-4.

Cao, Guangchao, Hua Bing Li, Zhinan Yin, and Richard A. Flavell. 2016. 'Recent Advances in Dynamic M6A RNA Modification'. *Open Biology* 6 (4): 1–8. https://doi.org/10.1098/rsob.16.0003.

Capitanchik, Charlotte, Patrick Toolan-Kerr, Nicholas M. Luscombe, and Jernej Ule. 2020. 'How Do You Identify M6 A Methylation in Transcriptomes at High Resolution? A Comparison of Recent Datasets'. *Frontiers in Genetics* 11 (May): 1–12. https://doi.org/10.3389/fgene.2020.00398.

Carneiro, Benedito A., and Wafik S. El-Deiry. 2020. 'Targeting Apoptosis in Cancer Therapy'. *Nature Reviews Clinical Oncology* 17 (7): 395–417. https://doi.org/10.1038/s41571-020-0341-y.

Choe, Junho, Shuibin Lin, Wencai Zhang, Qi Liu, Longfei Wang, Julia Ramirez-Moya, Peng Du, et al. 2018. 'MRNA Circularization by METTL3–EIF3h Enhances Translation and Promotes Oncogenesis'. *Nature* 561 (7724): 556–60. https://doi.org/10.1038/s41586-018-0538-8.

Cohn, W. E. 1960. 'Pseudouridine, a Carbon-Carbon Linked Ribonucleoside in Ribonucleic Acids: Isolation, Structure, and Chemical Characteristics.' *The Journal*

of Biological Chemistry 235 (5): 1488–98. https://doi.org/10.1016/s0021-9258(18)69432-3.

Davis, F. F., and F. W. Allen. 1957. 'Ribonucleic Acids from Yeast Which Contain a Fifth Nucleotide'. *The Journal of Biological Chemistry* 227 (2): 907–15. https://doi.org/10.1016/s0021-9258(18)70770-9.

Desrosiers, R., K. Friderici, and F. Rottman. 1974. 'Identification of Methylated Nucleosides in Messenger RNA from Novikoff Hepatoma Cells'. *Proceedings of the National Academy of Sciences of the United States of America* 71 (10): 3971–75. https://doi.org/10.1073/pnas.71.10.3971.

Dominissini, Dan, Sharon Moshitch-Moshkovitz, Schraga Schwartz, Mali Salmon-Divon, Lior Ungar, Sivan Osenberg, Karen Cesarkas, et al. 2012. 'Topology of the Human and Mouse M6A RNA Methylomes Revealed by M6A-Seq'. *Nature* 485 (7397): 201–6. https://doi.org/10.1038/nature11112.

Elmore, Susan. 2007. 'Apoptosis: A Review of Programmed Cell Death'. *Toxicologic Pathology* 35 (4): 495–516. https://doi.org/10.1080/01926230701320337.

Garcia-Campos, Miguel Angel, Sarit Edelheit, Ursula Toth, Modi Safra, Ran Shachar, Sergey Viukov, Roni Winkler, et al. 2019. 'Deciphering the "M6A Code" via Antibody-Independent Quantitative Profiling'. *Cell* 178 (3): 731-747.e16. https://doi.org/10.1016/j.cell.2019.06.013.

Greenbaum, Dov, Christopher Colangelo, Kenneth Williams, and Mark Gerstein. 2003. 'Comparing Protein Abundance and MRNA Expression Levels on a Genomic Scale'. *Genome Biology* 4 (9). https://doi.org/10.1186/gb-2003-4-9-117.

Grosjean, Henri. 2005. 'Modification and Editing of RNA: Historical Overview and Important Facts to Remember' 12 (January): 1–22. https://doi.org/10.1007/b106848.

Gupta, S. 2005. 'Molecular Steps of Tumor Necrosis Factor Receptor-Mediated Apoptosis'. *Current Molecular Medicine* 1 (3): 317–24. https://doi.org/10.2174/1566524013363780.

Guttman, Mitchell, and John L. Rinn. 2012. 'Modular Regulatory Principles of Large Non–Coding RNAs'. *Nature* 482 (7385): 339–46. https://doi.org/10.1038/nature10887.Modular.

Haussmann, Irmgard U., Zsuzsanna Bodi, Eugenio Sanchez-Moran, Nigel P. Mongan, Nathan Archer, Rupert G. Fray, and Matthias Soller. 2016. 'M6 A Potentiates Sxl Alternative Pre-MRNA Splicing for Robust Drosophila Sex Determination'. *Nature*

540 (7632): 301–4. https://doi.org/10.1038/nature20577.

He, Liuer, Huiyu Li, Anqi Wu, Yulong Peng, Guang Shu, and Gang Yin. 2019. 'Functions of N6-Methyladenosine and Its Role in Cancer'. *Molecular Cancer* 18 (1): 1–15. https://doi.org/10.1186/s12943-019-1109-9.

He, P Cody, and Chuan He. 2021. ' M 6 A RNA Methylation: From Mechanisms to Therapeutic Potential '. *The EMBO Journal* 40 (3): 1–15. https://doi.org/10.15252/embj.2020105977.

Holbrook, Jonathan, Samuel Lara-Reyna, Heledd Jarosz-Griffiths, and Michael McDermott. 2019. 'Tumour Necrosis Factor Signalling in Health and Disease [Version 1; Referees: 2 Approved]'. *F1000Research* 8 (January). https://doi.org/10.12688/f1000research.17023.1.

Horssen, Remco van, Timo L. M. ten Hagen, and Alexander M. M. Eggermont. 2006. 'TNF-α in Cancer Treatment: Molecular Insights, Antitumor Effects, and Clinical Utility'. *The Oncologist* 11 (4): 397–408. https://doi.org/10.1634/theoncologist.11-4-397.

Hotchkiss, D. 1948. 'THE QUANTITATIVE SEPARATION OF PURINES , SND NUCLEOSIDES BY The Separation of Amino Acid Mixtures by Migration with Organic Solvents in Filter Paper Has Been Successfully Accomplished by Many Workers since It Was First Described by Consden , Gordon , And '. *Journal of Biological Chemistry* 175 (1): 315–32. https://doi.org/10.1016/S0021-9258(18)57261-6.

Hotchkiss, Richard S., Andreas Strasser, Jonathan E. McDunn, and Paul E. Swanson. 2009. 'Cell Death'. *The New England Journal of Medicine*.

Hsu, Phillip J., Hailing Shi, Allen C. Zhu, Zhike Lu, Nimrod Miller, Brittany M. Edens, Yongchao C. Ma, and Chuan He. 2019. 'The RNA-Binding Protein FMRP Facilitates the Nuclear Export of N6-Methyladenosine–Containing MRNAs'. *Journal of Biological Chemistry* 294 (52): 19889–95. https://doi.org/10.1074/jbc.AC119.010078.

Hu, Xiaoge, Wan Xin Peng, Huaixiang Zhou, Jiahong Jiang, Xinchun Zhou, Dongsheng Huang, Yin Yuan Mo, and Liu Yang. 2020. 'IGF2BP2 Regulates DANCR by Serving as an N6-Methyladenosine Reader'. *Cell Death and Differentiation* 27 (6): 1782–94. https://doi.org/10.1038/s41418-019-0461-z.

Huang, Huilin, Hengyou Weng, Wenju Sun, Xi Qin, Hailing Shi, Huizhe Wu, Boxuan

Simen Zhao, et al. 2018. ‘Recognition of RNA N 6 -Methyladenosine by IGF2BP Proteins Enhances MRNA Stability and Translation’. *Nature Cell Biology* 20 (3): 285–95. https://doi.org/10.1038/s41556-018-0045-z.

Huang, Jinbo, and Ping Yin. 2018. ‘Structural Insights into N6-Methyladenosine (M6A) Modification in the Transcriptome’. *Genomics, Proteomics and Bioinformatics* 16 (2): 85–98. https://doi.org/10.1016/j.gpb.2018.03.001.

Huang, Yue, Rui Su, Yue Sheng, Lei Dong, Ze Dong, Hongjiao Xu, Tengfeng Ni, et al. 2019. ‘Small-Molecule Targeting of Oncogenic FTO Demethylase in Acute Myeloid Leukemia’. *Cancer Cell* 35 (4): 677-691.e10. https://doi.org/10.1016/j.ccell.2019.03.006.

Imanishi, Miki, Shogo Tsuji, Akiyo Suda, and Shiroh Futaki. 2017. ‘Detection of: N 6-Methyladenosine Based on the Methyl-Sensitivity of MazF RNA Endonuclease’. *Chemical Communications* 53 (96): 12930–33. https://doi.org/10.1039/c7cc07699a.

Jan, Rehmat, and Gul-e-Saba Chaudhry. 2019. ‘Understanding Apoptosis and Apoptotic Pathways Targeted Cancer Therapeutics’. *Advanced Pharmaceutical Bulletin* 9 (2): 203–18. https://doi.org/10.15171/jcvtr.2015.24.

Janus, Patryk, Katarzyna Mrowiec, Natalia Vydra, Piotr Widłak, Agnieszka Toma-Jonik, Joanna Korfanty, Ryszard Smolarczyk, and Wiesława Widłak. 2020. ‘PHLDA1 Does Not Contribute Directly to Heat Shock-Induced Apoptosis of Spermatocytes’. *International Journal of Molecular Sciences* 21 (1): 1–10. https://doi.org/10.3390/ijms21010267.

Julien, Olivier, and James A. Wells. 2017. ‘Caspases and Their Substrates’. *Cell Death and Differentiation* 24 (8): 1380–89. https://doi.org/10.1038/cdd.2017.44.

Kaczanowski, Szymon. 2016. ‘Apoptosis: Its Origin, History, Maintenance and the Medical Implications for Cancer and Aging’. *Physical Biology* 13 (3). https://doi.org/10.1088/1478-3975/13/3/031001.

Kaya-Aksoy, Ezgi, Ahmet Cingoz, Filiz Senbabaoglu, Fidan Seker, Ilknur Sur-Erdem, Alisan Kayabolen, Tolga Lokumcu, Gizem Nur Sahin, Sercin Karahuseyinoglu, and Tugba Bagci-Onder. 2019. ‘The Pro-Apoptotic Bcl-2 Family Member Harakiri (HRK) Induces Cell Death in Glioblastoma Multiforme’. *Cell Death Discovery* 5 (1). https://doi.org/10.1038/s41420-019-0144-z.

Kerr J. F. R., Wyllie A. H., Currie a. R. 1972. ‘Apoptosis : A Basic Biological Phenomenon With Wide-’. *Br. J. Cancer* 26: 239–57.

Klanova, Magdalena, and Pavel Klener. 2020. 'BCL-2 Proteins in Pathogenesis and Therapy of B-Cell Non-Hodgkin Lymphomas'. *Cancers* 12 (4): 1–21. https://doi.org/10.3390/cancers12040938.

Kretschmer, Jens, Harita Rao, Philipp Hackert, Katherine E. Sloan, Claudia Höbartner, and Markus T. Bohnsack. 2018. 'The M6A Reader Protein YTHDC2 Interacts with the Small Ribosomal Subunit and the 5′-3′ Exoribonuclease XRN1'. *Rna* 24 (10): 1339–50. https://doi.org/10.1261/rna.064238.117.

Kurosaka, Kahori, Munehisa Takahashi, Naoko Watanabe, and Yoshiro Kobayashi. 2003. 'Silent Cleanup of Very Early Apoptotic Cells by Macrophages'. *The Journal of Immunology* 171 (9): 4672–79. https://doi.org/10.4049/jimmunol.171.9.4672.

'Li2016.Pdf'. n.d.

Lin, Sen, Jianing Liu, Wen Jiang, Peng Wang, Chao Sun, Xuexiang Wang, Yuan Chen, and Hongbo Wang. 2019. 'METTL3 Promotes the Proliferation and Mobility of Gastric Cancer Cells'. *Open Medicine (Poland)* 14 (1): 25–31. https://doi.org/10.1515/med-2019-0005.

Lin, Shuibin, Junho Choe, Peng Du, Robinson Triboulet, and Richard I. Gregory. 2016. 'The M6A Methyltransferase METTL3 Promotes Translation in Human Cancer Cells'. *Molecular Cell* 62 (3): 335–45. https://doi.org/10.1016/j.molcel.2016.03.021.

Linder, Bastian, Anya V. Grozhik, Anthony O. Olarerin-George, Cem Meydan, Christopher E. Mason, and Samie R. Jaffrey. 2015. 'Single-Nucleotide-Resolution Mapping of M6A and M6Am throughout the Transcriptome'. *Nature Methods* 12 (8): 767–72. https://doi.org/10.1038/nmeth.3453.

Liu, Jiqin, Dangli Ren, Zhenhua Du, Hekong Wang, Hua Zhang, and Ying Jin. 2018. 'M6A Demethylase FTO Facilitates Tumor Progression in Lung Squamous Cell Carcinoma by Regulating MZF1 Expression'. *Biochemical and Biophysical Research Communications* 502 (4): 456–64. https://doi.org/10.1016/j.bbrc.2018.05.175.

Liu, Shuiping, Lvjia Zhuo, Jianjun Wang, Qin Zhang, Qiujie Li, Guohua Li, Lili Yan, et al. 2020. 'METTL3 Plays Multiple Functions in Biological Processes.' *American Journal of Cancer Research* 10 (6): 1631–46. http://www.ncbi.nlm.nih.gov/pubmed/32642280%0Ahttp://www.pubmedcentral.nih.gov/articlerender.fcgi?artid=PMC7339281.

Liu, Weiliang, Jingli Yan, Zhenhao Zhang, Hongru Pian, Chenghui Liu, and Zhengping Li. 2018. 'Identification of a Selective DNA Ligase for Accurate Recognition and Ultrasensitive Quantification of: N 6-Methyladenosine in RNA at One-Nucleotide Resolution'. *Chemical Science* 9 (13): 3354–59. https://doi.org/10.1039/c7sc05233b.

Macewan, David J. 2002. '<135-0704549a.Pdf>'.

Mahmood, Tahrin, and Ping Chang Yang. 2012. 'Western Blot: Technique, Theory, and Trouble Shooting'. *North American Journal of Medical Sciences* 4 (9): 429–34. https://doi.org/10.4103/1947-2714.100998.

Micheau, Olivier, and Jürg Tschopp. 2003. 'Induction of TNF Receptor I-Mediated Apoptosis via Two Sequential Signaling Complexes'. *Cell* 114 (2): 181–90. https://doi.org/10.1016/S0092-8674(03)00521-X.

Nachtergaele, Sigrid, and Chuan He. 2018. 'Chemical Modifications in the Life of an MRNA Transcript'. *Annual Review of Genetics* 52 (September): 349–72. https://doi.org/10.1146/annurev-genet-120417-031522.

Niu, Yamei, Xu Zhao, Yong Sheng Wu, Ming Ming Li, Xiu Jie Wang, and Yun Gui Yang. 2013. 'N6-Methyl-Adenosine (M6A) in RNA: An Old Modification with A Novel Epigenetic Function'. *Genomics, Proteomics and Bioinformatics* 11 (1): 8–17. https://doi.org/10.1016/j.gpb.2012.12.002.

Perry, R. P., and D. E. Kelley. 1974. 'Existence of Methylated Messenger RNA in Mouse L Cells'. *Cell* 1 (1): 37–42. https://doi.org/10.1016/0092-8674(74)90153-6.

Ping, Xiao Li, Bao Fa Sun, Lu Wang, Wen Xiao, Xin Yang, Wen Jia Wang, Samir Adhikari, et al. 2014. 'Mammalian WTAP Is a Regulatory Subunit of the RNA N6-Methyladenosine Methyltransferase'. *Cell Research* 24 (2): 177–89. https://doi.org/10.1038/cr.2014.3.

Pistritto, Giuseppa, Daniela Trisciuoglio, Claudia Ceci, Alessia Garufi, and Gabriella D'Orazi. 2016. 'Apoptosis as Anticancer Mechanism: Function and Dysfunction of Its Modulators and Targeted Therapeutic Strategies'. *Aging* 8 (4): 603–19. https://doi.org/10.18632/aging.100934.

Qi, Yiming, Ying Li, Yingke Zhang, Lin Zhang, Zilian Wang, Xuzhi Zhang, Lian Gui, and Junqi Huang. 2015. 'IFI6 Inhibits Apoptosis via Mitochondrial-Dependent Pathway in Dengue Virus 2 Infected Vascular Endothelial Cells'. *PLoS ONE* 10 (8): 1–14. https://doi.org/10.1371/journal.pone.0132743.

Qian, Jia Yi, Jian Gao, Xi Sun, Meng Da Cao, Liang Shi, Tian Song Xia, Wen Bin Zhou, Shui Wang, Qiang Ding, and Ji Fu Wei. 2019. 'KIAA1429 Acts as an Oncogenic Factor in Breast Cancer by Regulating CDK1 in an N6-Methyladenosine-Independent Manner'. *Oncogene* 38 (33): 6123–41. https://doi.org/10.1038/s41388-019-0861-z.

Rah, Bilal, Reyaz ur Rasool, Debasis Nayak, Syed Khalid Yousuf, Debaraj Mukherjee, Lekha Dinesh Kumar, and Anindya Goswami. 2015. 'PAWR-Mediated Suppression of BCL2 Promotes Switching of 3-Azido Withaferin A (3-AWA)-Induced Autophagy to Apoptosis in Prostate Cancer Cells'. *Autophagy* 11 (2): 314–31. https://doi.org/10.1080/15548627.2015.1017182.

Rath, Pramod C., and Bharat B. Aggarwal. 1999. 'TNF-Induced Signaling in Apoptosis'. *Journal of Clinical Immunology* 19 (6): 350–64. https://doi.org/10.1023/A:1020546615229.

Saletore, Yogesh, Kate Meyer, Jonas Korlach, Igor D Vilfan, Samie Jaffrey, and Christopher E Mason. 2012. 'The Birth of the Epitranscriptome: Deciphering the Function of RNA Modifications Yogesh'. *Genome Biology* 13 (175): 8–12. https://doi.org/10.1123/IJNS.V4I3.215.

Schöller, E V A, Franziska Weichmann, Thomas Treiber, S A M Ringle, Nora Treiber, Andrew Flatley, Regina Feederle, Astrid Bruckmann, and Gunter Meister. 2018. 'Interactions , Localization , and Phosphorylation of the m 6 A Generating METTL3 – METTL14 – WTAP Complex', 499–512. https://doi.org/10.1261/rna.064063.117.3.

Sedger, Lisa M., and Michael F. McDermott. 2014. 'TNF and TNF-Receptors: From Mediators of Cell Death and Inflammation to Therapeutic Giants - Past, Present and Future'. *Cytokine and Growth Factor Reviews* 25 (4): 453–72. https://doi.org/10.1016/j.cytogfr.2014.07.016.

Sivamani, Bibhas kar and S. 2015. 'Kar and Sivamani',. *International Journal of Pharmaceutical Sciences and Research* 6 (3): 940–50.

Slobodin, Boris, Ruiqi Han, Vittorio Calderone, Joachim A.F.Oude Vrielink, Fabricio Loayza-Puch, Ran Elkon, and Reuven Agami. 2017. 'Transcription Impacts the Efficiency of MRNA Translation via Co-Transcriptional N6-Adenosine Methylation'. *Cell* 169 (2): 326-337.e12. https://doi.org/10.1016/j.cell.2017.03.031.

Smaele, E. De, F. Zazzeroni, S. Papa, D. U. Nguyen, R. Jin, J. Jones, R. Cong, and G.

Franzoso. 2001. ‘Induction of Gadd4β by NF-KB Downregulates pro-Apoptotic JNK Signalling’. *Nature* 414 (6861): 308–13. https://doi.org/10.1038/35104560.

Song, Huiwen, Xing Feng, Heng Zhang, Yunmei Luo, Juan Huang, Meihua Lin, Junfei Jin, et al. 2019. ‘METTL3 and ALKBH5 Oppositely Regulate M6A Modification of TFEB MRNA, Which Dictates the Fate of Hypoxia/Reoxygenation-Treated Cardiomyocytes’. *Autophagy* 15 (8): 1419–37. https://doi.org/10.1080/15548627.2019.1586246.

Starr, J. L., and B. H. Sells. 1969. ‘Methylated Ribonucleic Acids.’ *Physiological Reviews* 49 (3): 623–69. https://doi.org/10.1152/physrev.1969.49.3.623.

Vu, Ly P., Brian F. Pickering, Yuanming Cheng, Sara Zaccara, Diu Nguyen, Gerard Minuesa, Timothy Chou, et al. 2017. ‘The N 6 -Methyladenosine (m 6 A)-Forming Enzyme METTL3 Controls Myeloid Differentiation of Normal Hematopoietic and Leukemia Cells’. *Nature Medicine* 23 (11): 1369–76. https://doi.org/10.1038/nm.4416.

Wajant, Harald, and Daniela Siegmund. 2019. ‘TNFR1 and TNFR2 in the Control of the Life and Death Balance of Macrophages’. *Frontiers in Cell and Developmental Biology* 7 (May): 1–14. https://doi.org/10.3389/fcell.2019.00091.

Wang, Hong, Bei Xu, and Jun Shi. 2020. ‘N6-Methyladenosine METTL3 Promotes the Breast Cancer Progression via Targeting Bcl-2’. *Gene* 722 (August 2019): 144076. https://doi.org/10.1016/j.gene.2019.144076.

Wang, Xiao, and Chuan He. 2014. ‘Reading RNA Methylation Codes through Methyl-Specific Binding Proteins’. *RNA Biology* 11 (6). https://doi.org/10.4161/rna.28829.

Wei, Wenwen, Baosheng Huo, and Xiulan Shi. 2019. ‘MiR-600 Inhibits Lung Cancer via Downregulating the Expression of METTL3’. *Cancer Management and Research* 11: 1177–87. https://doi.org/10.2147/CMAR.S181058.

Wiener, David, and Schraga Schwartz. 2021. ‘The Epitranscriptome beyond M6A’. *Nature Reviews Genetics* 22 (2): 119–31. https://doi.org/10.1038/s41576-020-00295-8.

Xiao, Yu, Ye Wang, Qian Tang, Lianhuan Wei, Xiao Zhang, and Guifang Jia. 2018. ‘An Elongation- and Ligation-Based QPCR Amplification Method for the Radiolabeling-Free Detection of Locus-Specific N6-Methyladenosine Modification’. *Angewandte Chemie - International Edition* 57 (49): 15995–0. https://doi.org/10.1002/anie.201807942.

Xu, Feiyue, Chi Han Li, Chi Hin Wong, George G. Chen, Paul Bo San Lai, Shengwen Shao, Stephen L. Chan, and Yangchao Chen. 2019. 'Genome-Wide Screening and Functional Analysis Identifies Tumor Suppressor Long Noncoding RNAs Epigenetically Silenced in Hepatocellular Carcinoma'. *Cancer Research* 79 (7): 1305–17. https://doi.org/10.1158/0008-5472.CAN-18-1659.

Xu, Guangwu, and Yufang Shi. 2007. 'Apoptosis Signaling Pathways and Lymphocyte Homeostasis'. *Cell Research* 17 (9): 759–71. https://doi.org/10.1038/cr.2007.52.

Zaccara, Sara, and Samie R Jaffrey. 2020. 'Article A Unified Model for the Function of YTHDF Proteins in Regulating m 6 A-Modified MRNA Article A Unified Model for the Function of YTHDF Proteins in Regulating m 6 A-Modified MRNA'. *Cell*, 1–14. https://doi.org/10.1016/j.cell.2020.05.012.

Zaccara, Sara, Ryan J. Ries, and Samie R. Jaffrey. 2019. 'Reading, Writing and Erasing MRNA Methylation'. *Nature Reviews Molecular Cell Biology* 20 (10): 608–24. https://doi.org/10.1038/s41580-019-0168-5.

Zhang, Yuhao, Xiuchao Geng, Qiang Li, Jianglong Xu, Yanli Tan, Menglin Xiao, Jia Song, Fulin Liu, Chuan Fang, and Hong Wang. 2020. 'M6A Modification in RNA: Biogenesis, Functions and Roles in Gliomas'. *Journal of Experimental and Clinical Cancer Research* 39 (1): 1–16. https://doi.org/10.1186/s13046-020-01706-8.

Zhu, Wei, Jing Zi Wang, Zhiqiang Xu, Mengda Cao, Qiaoli Hu, Chen Pan, Miao Guo, Ji Fu Wei, and Haiwei Yang. 2019. 'Detection of N 6 -methyladenosine Modification Residues (Review)'. *International Journal of Molecular Medicine* 43 (6): 2267–78. https://doi.org/10.3892/ijmm.2019.4169.